Article

Neuron

Axonal Degeneration Is Regulated by a Transcriptional Program that Coordinates Expression of Pro- and Anti-degenerative Factors

Highlights

- Ablation of DUSP16, a dual phosphatase, accelerates axonal degeneration
- DUSP16 is required for sensory axon preservation during development
- DUSP16 negatively regulates the expression of the pro-degenerative factor PUMA
- Co-ablation of PUMA with DUSP16 protects from accelerated axonal degeneration

Authors

Maya Maor-Nof, Erez Romi, Hadas Sar Shalom, ..., Dena Leshkowitz, Roland Lang, Avraham Yaron

Correspondence

avraham.yaron@weizmann.ac.il

In Brief

Moar-Nof et al. describe the identification of the dual specificity phosphatase DUSP16 as a new axonal protective factor. They show that DUSP16 inhibits the expression of the pro-degenerative factor PUMA, which is required for axonal degeneration.

Accession Numbers

GSE72129

Maor-Nof et al., 2016, Neuron *92*, 991–1006
December 7, 2016
http://dx.doi.org/10.1016/j.neuron.2016.10.061

CellPress

Neuron
Article

Axonal Degeneration Is Regulated by a Transcriptional Program that Coordinates Expression of Pro- and Anti-degenerative Factors

Maya Maor-Nof,[1] Erez Romi,[1] Hadas Sar Shalom,[1] Valeria Ulisse,[1] Calanit Raanan,[2] Aviv Nof,[3] Dena Leshkowitz,[4] Roland Lang,[5] and Avraham Yaron[1,6,*]
[1]Department of Biomolecular Sciences
[2]Department of Veterinary Resources
Weizmann Institute of Science, Rehovot 76100, Israel
[3]Hazyar Zvi Shur 27 Petach Tikva 4921041, Israel
[4]Bioinformatics Unit, Life Sciences Core Facilities, Weizmann Institute of Science, Rehovot 76100, Israel
[5]Institute of Clinical Microbiology, Immunology and Hygiene, University Hospital Erlangen, Friedrich-Alexander-Universität Erlangen-Nürnberg, 91054 Erlangen, Germany
[6]Lead Contact
*Correspondence: avraham.yaron@weizmann.ac.il
http://dx.doi.org/10.1016/j.neuron.2016.10.061

SUMMARY

Developmental neuronal cell death and axonal elimination are controlled by transcriptional programs, of which their nature and the function of their components remain elusive. Here, we identified the dual specificity phosphatase Dusp16 as part of trophic deprivation-induced transcriptome in sensory neurons. Ablation of *Dusp16* enhanced axonal degeneration in response to trophic withdrawal, suggesting that it has a protective function. Moreover, axonal skin innervation was severely reduced while neuronal elimination was increased in the *Dusp16* knockout. Mechanistically, Dusp16 negatively regulates the transcription factor p53 and antagonizes the expression of the pro-degenerative factor, Puma (p53 upregulated modulator of apoptosis). Co-ablation of *Puma* with *Dusp16* protected axons from rapid degeneration and specifically reversed axonal innervation loss early in development with no effect on neuronal deficits. Overall, these results reveal that physiological axonal elimination is regulated by a transcriptional program that integrates regressive and progressive elements and identify Dusp16 as a new axonal preserving factor.

INTRODUCTION

Trophic factors, of which nerve growth factor (NGF) is the founding member, are critical regulators of axonal maintenance and cell survival (Harrington and Ginty, 2013; Huang and Reichardt, 2001). Previous studies have identified trophic factor-induced genes that are critical for axon maintenance, including *Bcl-w*, *Impa1*, and *Lmnb2* (Andreassi et al., 2010; Courchesne et al., 2011; Tasdemir-Yilmaz and Segal, 2016; Yoon et al., 2012). Loss of trophic signaling was found to elicit transcriptional programs that govern neuronal death as well as axonal degeneration. Early studies using the developing chick embryo demonstrated that active transcription is required for cell death induced by ablation of the peripheral targets (Oppenheim et al., 1990). In later studies, the transcription factor c-Jun, members of the p53 family, and the transcriptionally induced BH3-only proteins *Hrk* and *Bim* were identified as key regulators of the apoptosis of sympathetic and dorsal root ganglion (DRG) neurons during development (Aloyz et al., 1998; Ham et al., 1995; Imaizumi et al., 1997; Putcha et al., 2001). Additional in vitro findings support the role of active gene transcription in neuronal cell death and axonal elimination following whole-culture trophic deprivation, since inhibiting transcription or translation preserved the neurons and their axons in culture (Martin et al., 1988). In addition, disconnection of axons from dying neurons protects the axons from degeneration. This supports the idea that mobilization of newly synthesized proteins from the cell body is required for axonal degeneration (Gerdts et al., 2013; Simon et al., 2016). However, to date, there has been no comprehensive analysis of this transcriptional program or functional analysis of its components.

Mechanisms that control axonal breakdown during development (axonal pruning) and after injury have begun to emerge in the last few years (Neukomm and Freeman, 2014; Pease and Segal, 2014; Schuldiner and Yaron, 2015). Components of the apoptotic system, including Caspases-9, -6, and -3, and the pro-apoptotic protein Bax, have been strongly implicated in axonal degeneration in response to trophic withdrawal in vitro and in axonal pruning in vivo (Maor-Nof and Yaron, 2013). Moreover, Caspases execute pruning of sensory neuron dendritic arbors during metamorphosis in *Drosophila* (Kuo et al., 2006; Williams et al., 2006), suggesting that the role of the apoptotic system in this developmental process is evolutionarily conserved. Interestingly, it was suggested that regulation of the apoptotic system in axons is distinct from that in cell bodies. Apaf-1 is critical for cell death but not for axonal degeneration, while

the Caspase inhibitor XIAP plays an important role in Caspase regulation in axons but not in the soma (Cusack et al., 2013; Unsain et al., 2013). However, other studies have challenged these findings (Simon et al., 2012, 2016). More recently, the pro-apoptotic protein Puma (p53 upregulated modulator of apoptosis) was found to elicit axonal degeneration through an unidentified anterograde degenerative program that activates the axonal apoptotic system (Simon et al., 2016).

We performed RNA sequencing (RNA-seq) analysis of sensory neurons following trophic deprivation in vitro to uncover the transcriptional program elicited in response to trophic withdrawal and to discover its role in axonal elimination. Dusp16 is upregulated in this paradigm and was selected for further study since its role in the nervous system has never been explored before. Our findings indicate that Dusp16 provides a safeguard mechanism to down-modulate the transcription upregulation of the pro-degenerative Puma, regulating axonal degeneration.

RESULTS

Uncovering a Trophic Withdrawal-Induced Transcriptional Program in Sensory Neurons

The ability of RNA and protein synthesis inhibitors to delay axonal degeneration and cell death of NGF-deprived sensory neurons in vitro (Martin et al., 1988) and to delay cell death of sensory and motor neurons in vivo (Oppenheim et al., 1990) suggested the existence of a transcriptional program that promotes cell death and axonal degeneration. To explore this in sensory neurons, we first determined the time point after trophic withdrawal at which the transcriptional program required for degeneration is completed. For this, we cultured DRG neurons from embryonic day 13.5 (E13.5) mice for 36 hr in the presence of NGF and applied the transcription inhibitor actinomycin D at different times after trophic withdrawal. Axonal degeneration magnitude was assessed after 24 hr. Inhibiting transcription within 6 hr after trophic withdrawal provided robust protection against axonal degeneration as monitored by microtubule (MT) depolymerization (Figures 1A–1D, 1F–1I, and 1K) and degradation of neurofilaments (NF) (Figures 1L and 1M). Addition of actinomycin D at later time points had some inhibitory effect, but this was much less profound (Figures 1E, 1J, and 1K). These data suggest that, after 6 hr, most of the transcriptional program that mediates axonal degeneration has been executed.

To identify and characterize components of the transcriptional program that initiates axonal degradation, we cultured DRG neurons for 36 hr in the presence of NGF and then induced deprivation. RNA was extracted after 1, 3, or 6 hr of trophic deprivation, and the neurons were subjected to RNA-seq analysis (Figure 2A). Transcriptional profiling demonstrated significant changes in gene expression after 3 hr and 6 hr of trophic deprivation relative to control cultures (control, 6 hr) (Figure 2B). These changes included increased expression of two genes previously reported to be induced in sensory neurons upon trophic deprivation, *Hrk* and *Jun* (increased by 6-fold and 2.7-fold, respectively). Using a 1.5-fold change as the threshold, 208 genes were found to be downregulated and 87 genes were upregulated. Using the CLICK algorithm (Sharan and Shamir, 2000) (Figure 2C), these genes were clustered with high homogeneity (>98) into four clusters based on the pattern of changes in their expression.

Analysis of this dataset using the Ingenuity Systems IPA platform suggested the emergence of an overall program representing a regressive process of neuronal cell bodies and their processes. Specifically, the group of induced genes was enriched in pathways that are generally involved in "cell death" of different cell types (11 genes). In contrast, the genes with reduced expression included pathways that participate in "cell survival" (54 genes) "development of neurons" (36 genes), "branching of neurons" (17 genes), "shape change of neurites" (17 genes), "branching of neurites (16 genes), and "neuritogenesis" (26 genes) (Table S1). This analysis provides a high-resolution dataset of changes in gene expression in sensory neurons upon trophic withdrawal.

Dusp16 Is a Negative Regulator of Axonal Degeneration and Caspase-3 Activation In Vitro

To begin to determine the functional implications of these transcriptional changes, we focused on the upregulated genes in clusters 3 and 4 (Figure 2C). Since our results showed that inhibition of transcription protects axons from degeneration, we hypothesized that genetic ablation of genes from these upregulated clusters would also confer axonal protection. Moreover, we aimed to analyze the genes that might converge to play a key role in regulating axonal degeneration during development and in the in vivo axonal response to injury. We therefore compared the upregulated genes from clusters 3 and 4 with those reported in two recently published gene-expression studies of axonal injury of retinal ganglion cells (RGCs) and DRGs (Michaelevski et al., 2010; Watkins et al., 2013).

We found only four genes, *Stmn4*, *Atf3*, *Dusp16*, and *Puma*, to be induced in all three datasets (Figure 2D), a highly significant intersection based on randomized test ($p < 0.001$). In a previous study, we used small interfering RNA (siRNA) to examine the role of Stmn4 and failed to detect a role for this protein in axonal degeneration following trophic deprivation (Maor-Nof et al., 2013). Atf3 is a known marker of axonal injury while the function of Dusp16 in the nervous system was not studied before (Niedzielska et al., 2014). We therefore decided to focus on Dusp16. Moreover, other members of the Dusp family are induced in response to trophic deprivation in different neurons, but their relative importance and specific functions are unknown (Kristiansen et al., 2011; Mariga et al., 2015). Using DRG neurons from *Dusp16* knockout (KO) mice, we first examined whether Dusp16 plays a role in axonal degeneration in response to trophic deprivation in vitro. To our surprise, we found that the degeneration of axons from these neurons is more rapid compared with that from neurons of their wild-type (WT) littermates (Figures 3A–3I), indicating that Dusp16 is a negative regulator of axonal degeneration.

Given the central role of Caspase-3 in the process of axonal degeneration (Cusack et al., 2013; Simon et al., 2012), we next wanted to know whether its regulation in *Dusp16* KO mice is altered. To this end, we made use of the filter culture system, enabling us to differentiate between the neuronal soma and the axons (Schoenmann et al., 2010) (Figures 3J and 3K). E13.5 embryonic DRGs from *Dusp16* KO mice and wild-type littermates

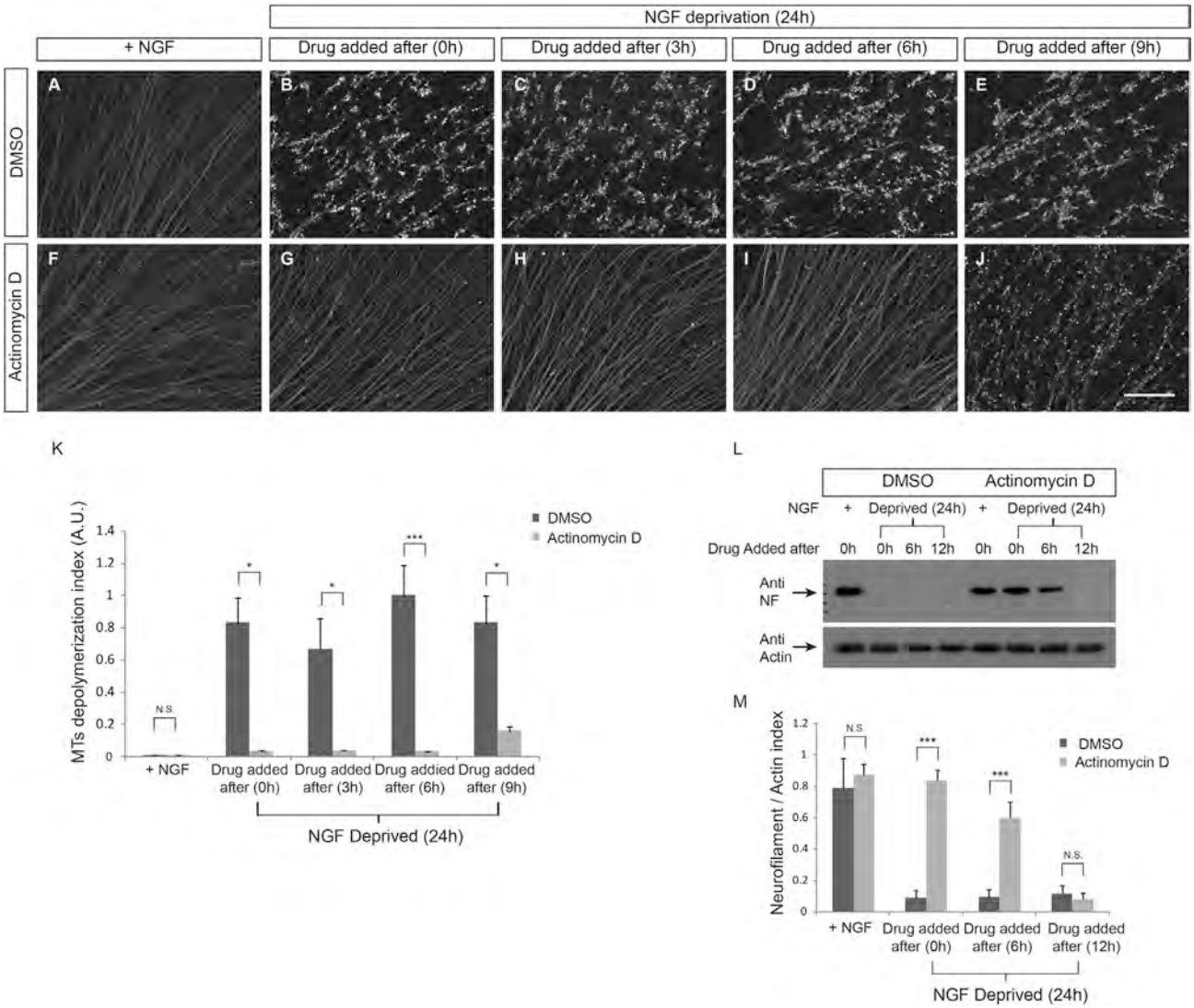

Figure 1. The Transcription Inhibitor Actinomycin D Protects against Axonal Degeneration Following NGF Deprivation

(A–K) DRG explants were cultured for 48 hr in NGF-containing medium and were either supplied with NGF (A and F) or deprived of NGF (B–E and G–J) for a further 24 hr and then immunostained for tubulin βIII. When deprived of NGF, axonal microtubules were depolymerized and degraded, as can be seen from the punctuated pattern of the microtubule staining (B–E). Axonal microtubules were protected from depolymerization by the addition of actinomycin D either before (0 hr) or up to 6 hr after NGF withdrawal (G–I). Addition of actinomycin D 9 hr post-NGF withdrawal did not protect against microtubule depolymerization (J). The extent of microtubule depolymerization (mean index ± SEM) was calculated for each condition (K), as described in the Supplemental Experimental Procedures (t test; ***$p < 0.001$, *$p < 0.05$, n.s., not significant). Scale bar, 100 μM.

(L and M) DRG explants were cultured for 36 hr in NGF-containing medium and then deprived of NGF for the next 24 hr. Actinomycin D or vehicle control (DMSO) was added upon NGF withdrawal (0 hr) or at 3, 6, or 9 hr following NGF withdrawal. Neurofilament degradation was assessed by immunoblot analysis (L). Neurofilaments were degraded after 24 hr of NGF deprivation but, like microtubules, were preserved by the addition of actinomycin D before (0 hr) or up to 6 hr after NGF withdrawal. Quantitation of neurofilament loss following NGF withdrawal was determined by immunoblots and normalized to actin (M). Graphs show mean ± SEM (t test; ***$p < 0.001$, n.s., $n = 4$).

were cultured for 48 hr on 1 μm filters, and trophic deprivation was induced for 8, 12, or 16 hr. Neuronal cell bodies and their axons were then extracted separately and subjected to biochemical analysis using anti-Caspase-3 antibody, which detects both the full Caspase-3 and its cleaved (active) short form. We found a pattern of trophic deprivation-induced Caspase-3 activation in both the cell bodies and the axons of *Dusp16* KO neurons, manifested by increases in the amount of the cleaved form (Figures 3L and 3M). Next, we tested the role of Caspase-3 activity in the more rapid axonal degeneration observed in *Dusp16* KO neurons. Although axonal degeneration was more advanced at 24 hr in *Dusp16* KO neurons than in wild-type neurons, 50 μM of the pan-Caspase inhibitor Z-VAD blocked axonal degeneration in a similar manner in both (Figures 3N–3V). These results suggest that ablation of *Dusp16* enhances Caspase-3 activation and axonal degeneration following trophic deprivation.

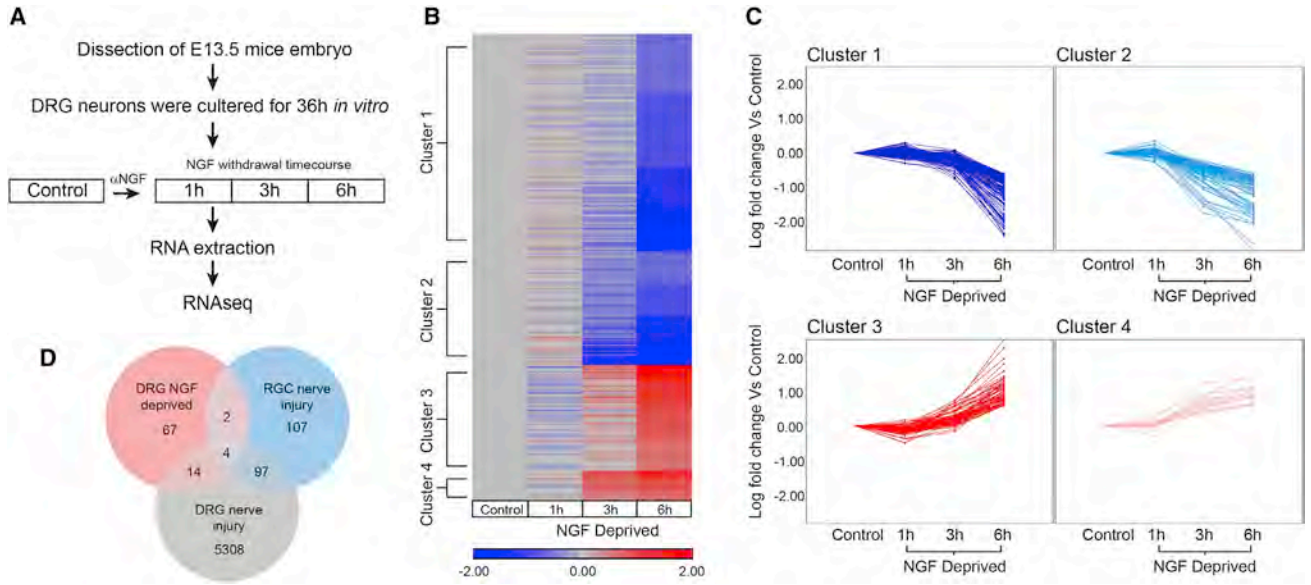

Figure 2. NGF Deprivation Induces a Transcriptional Program

(A) Schematic representation of the experimental paradigm used to uncover the transcriptional program induced by NGF withdrawal. Overall, 295 genes were significantly up- or downregulated at at least one time point in DRG neurons deprived of NGF for 1, 3, or 6 hr in comparison to control cells maintained in NGF. (B and C) Heatmap representation and clustering of the transcriptional program based on the log value of the ratio of gene expression in NGF-deprived DRGs to controls.

(D) 87 genes found to be significantly upregulated in the in vitro NGF-deprivation model in DRG neurons were compared to the genes upregulated following in vivo injury (crush) of optic nerve (RGC) and sciatic nerve (DRG). This comparison reveals that four genes were upregulated in all three models examined, a highly significant intersection based on randomized test ($p < 0.001$).

Decreased Axonal Branching and Target Innervation in the *Dusp16* KO Mice

We next examined the axonal protective role of Dusp16 in the development of the peripheral nervous system (PNS). Using whole-mount neurofilament staining, we studied the pattern of DRG axonal development at E12.5. The gross pattern of the axons in *Dusp16* KO embryos at that early stage was comparable to the pattern observed in their WT littermates (Figure S1). Moreover, DRG axons grow to the same extent in the *Dusp16* KO embryos as in their WT littermates. This suggested that Dusp16 does not regulate axonal growth or guidance (Figures 4A–4C). However, there was a clear reduction in the number of axonal branches (Figures 4A, 4B, and 4D), indicating that Dusp16 is a positive regulator of axonal morphogenesis. This finding is in line with its function as a negative regulator of axonal breakdown.

Next, we examined the innervation of the skin at E15.5. Strikingly, staining with the neuronal marker PGP9.5 (Figures 4E–4G) or the general axonal marker tubulin βIII (Figures 4H–4J) revealed approximately 50% fewer nerves innervating the skin in *Dusp16* KO mice than in WT controls. To examine the possibility that this strong reduction was due to massive cell death of DRG neurons with subsequent degeneration of their axons, we counted the cleaved Caspase-3-positive cells during development. Relative to controls, there is a 2.8-fold increase in the number of cleaved Caspase-3-positive cells at both E13.5 and E15.5 in the *Dusp16* KO mice (Figures 4K–4O). Consistent with this increase, the *Dusp16* KO mice exhibited a 16% reduction in the number of Islet1-positive DRG neurons at E13.5 and a 22% reduction at E15.5 (Figures 4P–4T). Taken together, these results support a critical role for Dusp16 in preserving sensory axons and, to a lesser extent, protecting the cell bodies during development.

Dusp16 Negatively Regulates the Expression of the Pro-apoptotic Protein Puma

Dusp16 has been shown to negatively regulate c-Jun N-terminal kinase (JNK) in the immune system (Niedzielska et al., 2014; Zhang et al., 2015). Moreover, the JNK pathway was found to control axonal degeneration and cell death in response to trophic withdrawal (Ghosh et al., 2011). We therefore examined the activation of JNK in response to trophic deprivation in DRG neurons of the *Dusp16* KO mice. Both in WT and in *Dusp16* KO neurons, an increase in JNK phosphorylation was detectable between 3 and 6 hr after NGF deprivation (Figures S2A–S2C). To our surprise, however, JNK activation was no greater in *Dusp16* KO neurons than in controls (Figures S2A–S2C). To verify these findings, we examined phosphorylation of the JNK substrate c-Jun, which is robustly induced in response to trophic withdrawal (Ghosh et al., 2011; Ham et al., 1995; Sun et al., 2005). The induction of c-Jun expression levels did not increase in the *Dusp16* KO neurons as compared to wild-type (Figures S2D–S2F). Consistent with our analysis of JNK activation, 6 hr of trophic deprivation induced c-Jun phosphorylation (pJun) to the same extent in both wild-type and *Dusp16* KO neurons (Figures S2D–S2F). Interestingly, at 9 hr post-deprivation, c-Jun phosphorylation falls in the *Dusp16* KO neurons but remains elevated in the

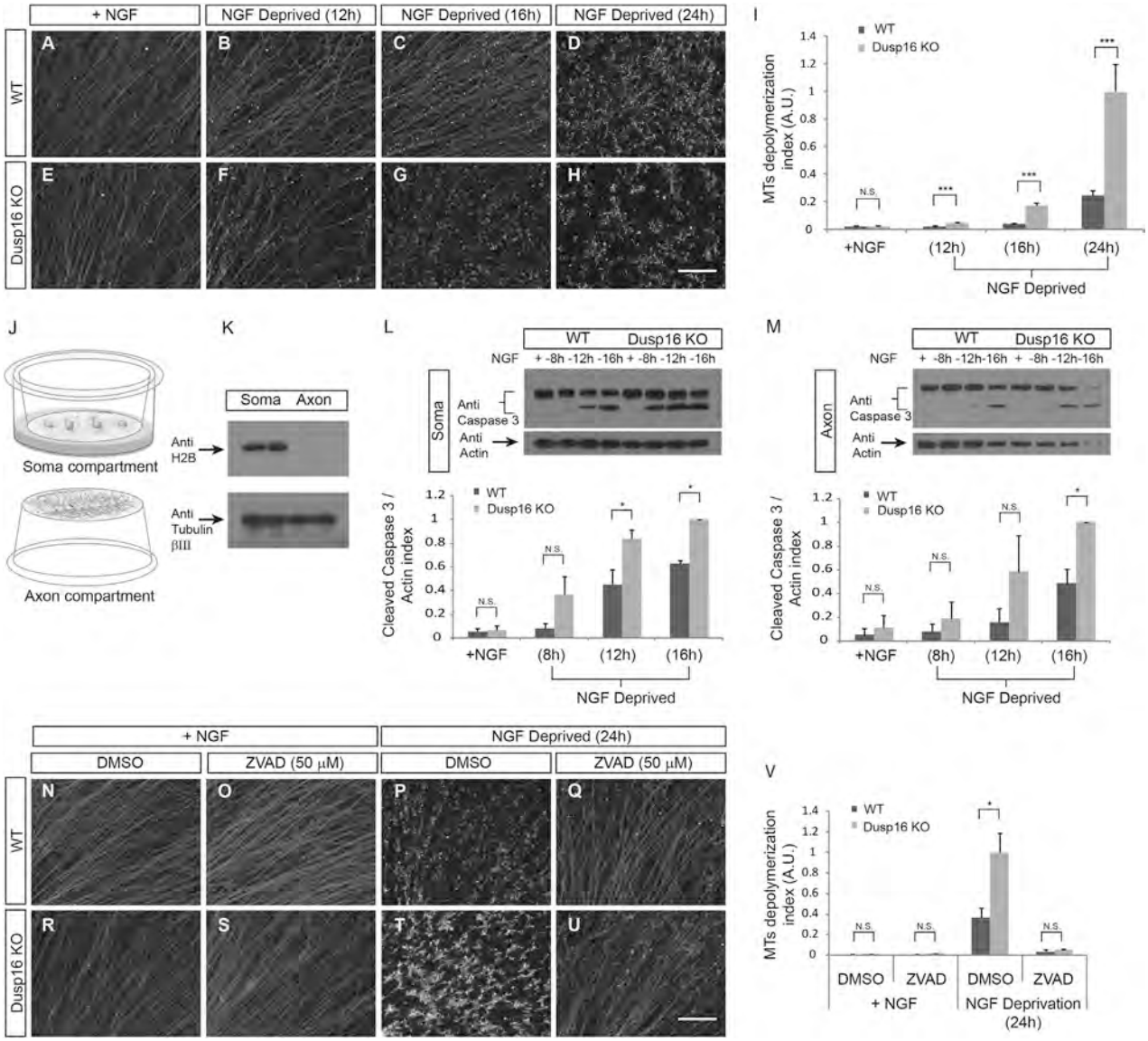

Figure 3. Genetic Ablation of *Dusp16* Enhances Microtubule Depolymerization upon NGF Deprivation

(A–I) DRG explants of either *Dusp16* KO embryos (E–H) or their WT littermates (A–D) were cultured for 48 hr in NGF-containing medium. These explants were either supplied with (A and E) or deprived of (B–D and F–H) NGF for an additional 12 hr (B and F), 16 hr (C and G), or 24 hr (D and H) and were then immunostained for tubulin βIII. Upon NGF deprivation, axonal microtubules (MTs) of the *Dusp16* KO neurons were depolymerized and degraded earlier and at a faster rate than the WT, as can be seen from the punctuated pattern of microtubule staining (F–H and B–D). Microtubule depolymerization (mean index ± SEM) was calculated for each condition and genotype (I) (t test; ***$p < 0.001$, n.s.). Scale bar, 100 μM.

(J) Schematic illustration of the insert cell culture system. The upper sketch shows the insert, plated with DRG neurons, inside a culture well. The lower sketch shows the underside of the insert, with axons that have passed through the 1 μm pores.

(K) Purity analysis of the axonal samples. DRG explants were grown in the presence of NGF for 36 hr on inserts, allowing the axons, but not the cell bodies, to pass through the 1 μm pores to the bottom side of the membrane. Axonal and somatic samples were collected separately. Biochemical analysis of these samples reveals the presence of histone H2B in the soma compartment only.

(L and M) Genetic ablation of *Dusp16* resulted in enhanced activation of Caspase-3 upon NGF deprivation. Activation of Caspase-3 was evaluated by immunoblot analysis; activated (cleaved) Caspase-3 appears as a second band below the uncleaved inactive Caspase-3 band. Enhanced appearance of the cleaved form is detected in the soma compartment (L) at 12 hr and 16 hr after NGF withdrawal and in the axonal compartment (M) after 16 hr. Quantitation of cleaved Caspase-3 following NGF withdrawal was determined by immunoblots and normalized to actin. Graphs show mean ± SEM (t test; *$p < 0.05$, n.s., $n = 3$).

(N–V) Caspase inhibitor blocks axonal degeneration in WT and *Dusp16* KO DRG neurons following NGF withdrawal. DRG explants of either *Dusp16* KO embryos (R–U) or their WT littermates (N–Q) were cultured for 48 hr in NGF-containing medium. These explants were either supplied with (N, O, R, and S) or deprived of (P, Q, T, and U) NGF for an additional 24 hr and were then immunostained for tubulin βIII. Axonal degeneration of both WT and *Dusp16* KO neurons was completely blocked by addition of the pan-Caspase inhibitor Z-VAD (Q and U). Microtubule depolymerization (mean index ± SEM) was calculated for each condition and genotype (V) (t test; *$p < 0.05$, n.s.). Scale bar, 100 μM.

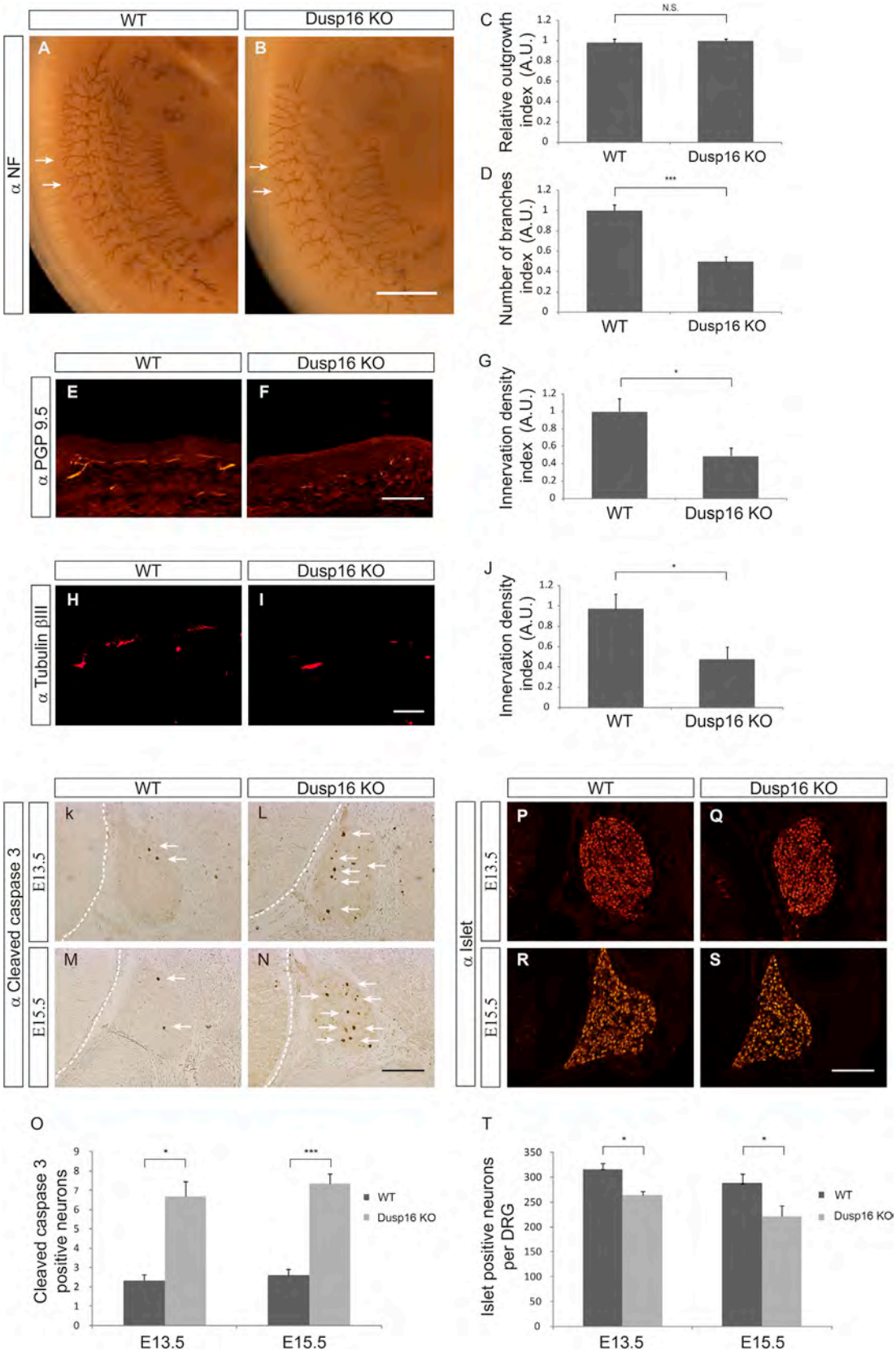

(legend on next page)

controls (Figures S2D–S2F). Overall, these results show that loss of Dusp16 has no effect on JNK activation in neurons following trophic deprivation. Similarly, we did not observe any change in activation of p38 in *Dusp16* KO neurons (Figures S2G–S2I). Our results indicate that the observed effects of *Dusp16* KO on axon degeneration are not mediated by increased activation of JNK/p38 signaling.

Since Puma is co-induced with Dusp16 in response to trophic deprivation and nerve injury (Figure 2D), we examined Puma expression. Upon NGF deprivation, Puma is transcriptionally upregulated as determined by our RNA-seq analysis. We then assessed Puma protein levels following trophic deprivation using the filter culture system described above (Figures 3J and 3K). Using a specific anti-Puma antibody, we detected induction of Puma in the soma compartment 8 hr and 12 hr after trophic deprivation (Figures 5A and 5B; Figure S2J). Importantly, Puma was also clearly detectable in the axonal compartment at these times points (Figures 5C and 5D). We next examined expression of Puma in *Dusp16* KO neurons in response to trophic withdrawal and observed more rapid induction of Puma (4 hr and 5 hr after NGF withdrawal) in *Dusp16* KO neurons than in control, suggesting that Dusp16 is an antagonist of Puma expression (Figures 5E and 5F). In contrast, *Puma* KO had no effect on the expression of Dusp16 in response to trophic withdrawal (Figure 5G). The transcriptional induction of Puma in response to multiple insults is controlled by p53 (Yu and Zhang, 2008), which is also important for cell death of sympathetic neurons and PC12 cells following NGF deprivation in vitro and during development in vivo (Aloyz et al., 1998; Vaghefi et al., 2004). p53 transcriptional activity is enhanced by phosphorylation on Ser15 (Loughery et al., 2014). Therefore, we examined the expression and the Ser15 phosphorylation status of p53 in response to trophic withdrawal in WT and *Dusp16* KO neurons. We did not detect an increase in p53 levels or of Foxo3a, which also regulates the transcription of *Puma*, following NGF deprivation at any time point tested (Figure 5H; Figures S2K, S2M, and S2N). In contrast, using a specific anti-pSer15 antibody, we detected an increase in p53 phosphorylation on Ser15 as early as 4 hr after trophic withdrawal (Figures 5I and 5J; Figure S2L). This phosphorylation was significantly enhanced in the *Dusp16* KO neurons at all tested time points (Figures 5I and 5J). In agreement with the role of Dusp16 as a negative regulator of p53 transcription activity, we found more rapid elevation of Puma mRNA in the *Dusp16* KO neurons compared with WT after trophic withdrawal (Figure 5K). These findings argue that Dusp16 in sensory neurons acts as a negative regulator of the apoptotic system, not via the JNK pathway, but by suppressing p53 transcriptional activity and thereby delaying Puma expression.

We next tested the upregulation of Puma in the *p53* KO neurons in response to NGF deprivation. The basal levels of Puma were not reduced in the *p53* KO neurons, but we detected a significant decrease in the induction of Puma in response to trophic withdrawal (Figures 5L and 5M), supporting the suggestion that p53 regulates the induction of Puma in response to trophic withdrawal. However, we detected no significant protection of axons in DRG explants from *p53* KO mice following trophic withdrawal (Figures S2O–S2S).

Puma Is Required for Efficient Axonal Degeneration and Restricts Axonal Branching and Target Innervation

Based on our observation of enhanced expression of Puma in *Dusp16* KO mice and its localization to the axons, we next examined the possible function of Puma in axonal degeneration. We cultured DRG explants from E13.5 WT and *Puma* KO embryos and induced axonal degeneration by whole-culture trophic deprivation. Microtubule breakdown following NGF deprivation was strongly attenuated in the Puma KO explants, as detected by anti-tubulin staining. While WT axons appeared completely degraded after 24 hr, in the Puma KO axons, depolymerization was detected mostly after 48 hr (Figures 6A–6I). Moreover, phase microscopy and biochemical analysis revealed complete axonal preservation of the Puma KO axons, complete preservation of the microtubules-associated protein Tau, and partial preservation of NF (Figures S3A–S3I). Biochemical analysis of Caspase-3 activation in DRG neurons of WT and *Puma* KO following NGF deprivation revealed a critical role for Puma in the activation of Caspase-3 in both cell bodies and axons (Figures S3J–S3M). To examine the role of Puma in local axonal degeneration and Caspase-3 activation directly, we used microfluidic chambers, in which NGF can be locally withdrawn from the axonal compartment while the cell bodies, maintained in the presence of NGF, remain intact (Figure 6J) (Cusack et al., 2013). Importantly, this local axonal degeneration also requires gene transcription (Chen et al., 2012). Using this system, we detected substantial preservation of axons in *Puma* KO neurons up to 72 hr after NGF withdrawal (Figures 6K and 6L). This protection was correlated with a lack of active Caspase-3, which exhibited a punctuated pattern in WT axons (Figures S3N and

Figure 4. *Dusp16* KO Mice Exhibit Reduced Axonal Branching, Reduced Target Innervation, and Enhanced Neuronal Cell Death

(A–D) Whole-mount NF staining of E12.5 *Dusp16* KO embryos and their WT littermates showing the peripheral nervous system growth pattern. The relative axonal outgrowth of *Dusp16* KO DRG spinal nerves does not differ from that of their WT littermates but exhibits significantly less branching (A and B, arrows). The relative outgrowth index of the DRG spinal nerves (C) and the axonal branches index of the DRG spinal nerves (D). Error bars represent means ± SEM (t test; ***$p < 0.001$; n.s., n = 4).

(E–J) Analysis of peripheral axons adjacent to the skin labeled with anti-PGP9.5 antibody (E–G) or anti-tubulin βIII antibody (H–J). Reduced innervation of sensory axons is detected in E15.5 *Dusp16* KO embryos (F and I) compared to their WT littermates (E and H). Innervation density index was determined by data collected from four embryos (40 sections each) of each genotype and is expressed as mean ± SEM (G and J) (t test; *$p < 0.05$).

(K–O) Increase in the number of Caspase-3-positive neurons in the DRGs of *Dusp16* KO embryos (L and N) in comparison to their WT littermates (K and M) at both E15.5 and E13.5. The mean (±SEM) number of cleaved Caspase-3-positive neurons per DRG was calculated by counting 40 sections per embryo in 3 to 4 embryos of each genotype (O) (t test; *$p < 0.05$, ***$p < 0.001$).

(P–T) The number of Islet1-positive neurons in the DRGs of *Dusp16* KO embryos is reduced (Q and S) in comparison to their WT littermates (P and R) at both E15.5 and E13.5. The number of Islet1-positive neurons was counted from 3 to 4 embryos (40 sections each) of each genotype and expressed as mean ± SEM (T) (t test; *$p < 0.05$). Scale bars, 1 mM (A and B), 100 μM (E, F, K–N, and P–S), and 50 μM (H and I).

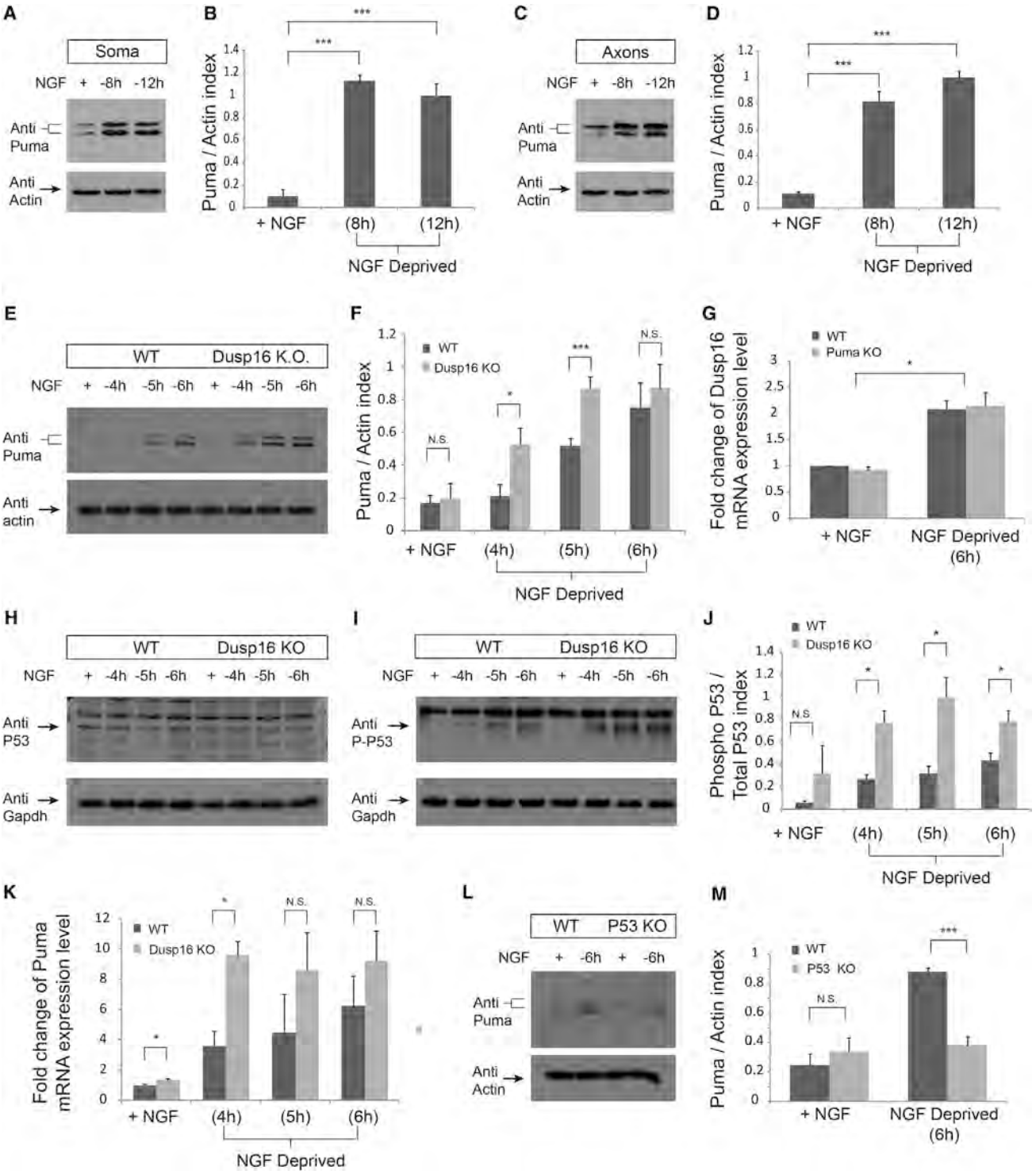

Figure 5. Genetic Ablation of *Dusp16* Induces Enhanced Phosphorylation of p53 and Rapid Expression of Puma

(A–D) DRG explants were grown in the presence of NGF for 36 hr on inserts, allowing the axons, but not the cell bodies, to pass through the 1 μm pores to the bottom side of the membrane. Cultures were deprived from NGF for 8 hr or 12 hr and Puma expression was analyzed in the soma (A) and the axonal (C) compartments by anti-Puma antibodies. Strong upregulation of Puma was detected in both compartments. Quantitation of Puma following NGF withdrawal was determined by immunoblots and normalized to actin (B and D). Graphs show mean ± SEM (t test; ***$p < 0.001$, $n = 3$).

(E and F) DRG explants from WT and *Dusp16* KO were cultured for 36 hr in NGF-containing medium and then deprived of NGF for the next 4, 5, or 6 hr. Puma was detected earlier in the *Dusp16* KO neurons, appearing at 4 hr, and at 5 hr, the Puma level in *Dusp16* KO neurons was significantly greater than in WT neurons (E).

(legend continued on next page)

S3O). Thus, in this in vitro paradigm, Puma appears to control Caspase-3 activation in axons.

Next, we examined the physiological role of Puma in PNS development. Using whole-mount NF staining at E12.5, we detected a minor (~16%), but significant, increase in axonal branching, with no change in extent of axonal growth in the *Puma* KO (Figures 6M–6P; Figures S3P and S3Q). We then examined the innervation of the skin at E15.5. In agreement with the axonal-destructive function of Puma, we detected hyperinnervation of the skin in the *Puma* KO mice embryos: a 90% increase using anti-PGP9.5 (Figures 6Q–6S) and a 40% increase using anti-tubulin βIII staining (Figures 6T–6V). This difference in the innervation quantification is due to the fact that anti-PGP9.5 staining reveals many small axonal branch fibers in the *Puma* KO that are not detected by the anti-βIII tubulin. We next examined the role of Puma in cell death and neuronal elimination. In agreement with our in vitro data, we detected a significant (~40%) reduction in the number of cleaved Caspase-3-positive cells in the Puma KO (Figures 6W–6Y), implying that Puma is required for efficient activation of Caspase-3 in neuronal cell bodies in vivo. However, the total number of DRG neurons (as determined by Islet1 staining) was not affected (Figures 6Z–6ZB). This indicates either that the reduced activation of Caspase-3 was still sufficient to eliminate neurons or, alternatively, that neurons were eliminated by a Caspase-3-independent death pathway that operates under physiological conditions (Yuan and Kroemer, 2010). These results support our findings in vitro, providing evidence that during development, Puma plays a more critical role in axonal breakdown than in neuronal cell death.

Co-ablation of *Puma* with *Dusp16* Inhibits Axonal Degeneration and Caspase-3 Activation

The above results suggest that Puma is required for axonal degeneration and is more rapidly induced in the *Dusp16* KO neurons. Therefore, we examined the function of Puma in the rapid axonal degeneration that we observed in the *Dusp16* KO neurons. We cultured DRG explants from E13.5 WT and *Dusp16*/*Puma* double KO embryos and induced axonal degeneration by trophic deprivation. We monitored axonal degeneration by anti-tubulin βIII staining and Caspase-3 activation by specifically staining for the cleaved active form. We observed a clear inhibition of axonal degeneration in the *Dusp16*/*Puma* KO compared to WT neurons (Figures 7A–7I and 7S–7Z). However, this inhibition of axonal degeneration was not to the same extent as in the *Puma* single KO (Figures 6E–6I). The slower axonal degeneration of the *Dusp16*/*Puma* double KO neurons was correlated with delayed activation of axonal Caspase-3 (Figures 7J–7Z). These results suggest that Puma is an important component of the axonal degeneration machinery operating downstream or in parallel to Dusp16.

Co-ablation of *Puma* with *Dusp16* Reverses the Reduction in Axonal Innervation, but Not Cell Death

Based on our observations that co-ablation of Puma with Dusp16 inhibits rapid axonal degradation following trophic deprivation in vitro, we examined whether the *Dusp16* KO phenotype is Puma dependent. For this, we analyzed the *Dusp16*/*Puma* double KO and all the single mutant controls at two developmental stages: E15.5, at the peak of neuronal cell death, and E17.5, when neuronal cell death is nearly complete (Piñon et al., 1996). We found a small, but significant, reduction in the number of cleaved Caspase-3-positive cells in DRGs in E15.5 *Dusp16*/*Puma* double KO embryos compared to *Dusp16* single KO embryos (Figures 8A–8E). However, the double KO still exhibited a 22% reduction in the number of Islet1-positive cells, identical to that seen in *Dusp16* KO embryos (Figures 8F–8J). These results suggest that Puma is not essential for neuronal elimination at this developmental stage, and *Puma* ablation cannot protect against increased cell death in the *Dusp16* KO. In striking contrast to the loss of neuronal cell bodies, we found that ablating Puma reversed the Dusp16 axonal phenotype: innervation in the double KO was indistinguishable from WT, as detected by both anti-PGP9.5 (Figures 8K–8O) and anti-tubulin βIII (Figures 8P–8T).

Developmental sensory neuron cell death is complete at E17.5 (Piñon et al., 1996). In agreement with this, we detected very few active Caspase-3-positive cells in WT embryos at this stage, and this number was not significantly different in *Puma* KO embryos. In contrast, we detected 2.5 times more active Caspase-3-positive cells in the *Dusp16* KO at this time point (Figures S4A–S4E). This number was markedly reduced compared to the number of Caspase-3-positive cells in the *Dusp16* KO at E13.5 and E15.5 (Figure 4; Figures S4A–S4E). Overall, neuronal number was reduced by 30% in the *Dusp16* KO (Figures S4F–S4J). Inspection of the axonal

Quantitation of Puma following NGF withdrawal was determined by immunoblots and normalized to actin (F). Graphs show mean ± SEM (t test; ***$p < 0.001$, *$p < 0.05$, n.s., n = 3).

(G) Expression of Dusp16 assayed by real-time PCR in DRG explants from WT and *Puma* KO. A 2-fold induction of Dusp16 mRNA expression levels was detected 6 hr after NGF deprivation in neurons of both genotypes (t test; *$p < 0.05$, n.s., n = 3).

(H–J) DRG explants from WT and *Dusp16* KO were cultured for 36 hr in NGF-containing medium and then deprived of NGF for the next 4, 5, or 6 hr. Total levels of p53 (H) and levels of p53 phosphorylated at Ser15 (I) were analyzed by immunoblots. The total p53 level did not change during this time course, but phosphorylation of p53 at Ser15 increased following NGF withdrawal in WT neurons and was further enhanced in the Dusp16 KO neurons (I and J). Quantitation of the ratio of phosphorylated p53 to total p53 following NGF withdrawal was determined by immunoblots and normalized to GAPDH (J). Graphs show mean ± SEM (t test; *$p < 0.05$, n.s., n = 3).

(K) Expression of Puma assayed by real-time PCR in DRG explants from WT and *Dusp16* KO. The expression of Puma mRNA increases more rapidly 4 hr after NGF deprivation in neurons of the *Dusp16* KO (t test; *$p < 0.05$, n.s., n = 3).

(L and M) DRG explants from WT and *p53* KO were cultured for 36 hr in NGF-containing medium and then deprived of NGF for 6 hr. The levels of Puma (L) were analyzed by immunoblots. Puma level was significantly increased following NGF withdrawal in WT neurons but not in the p53 KO neurons. Quantitation of the ratio of phosphorylated Puma to actin following NGF withdrawal was determined by immunoblots and normalized to GAPDH (M). Graphs show mean ± SEM (t test; ***$p < 0.01$, n = 3).

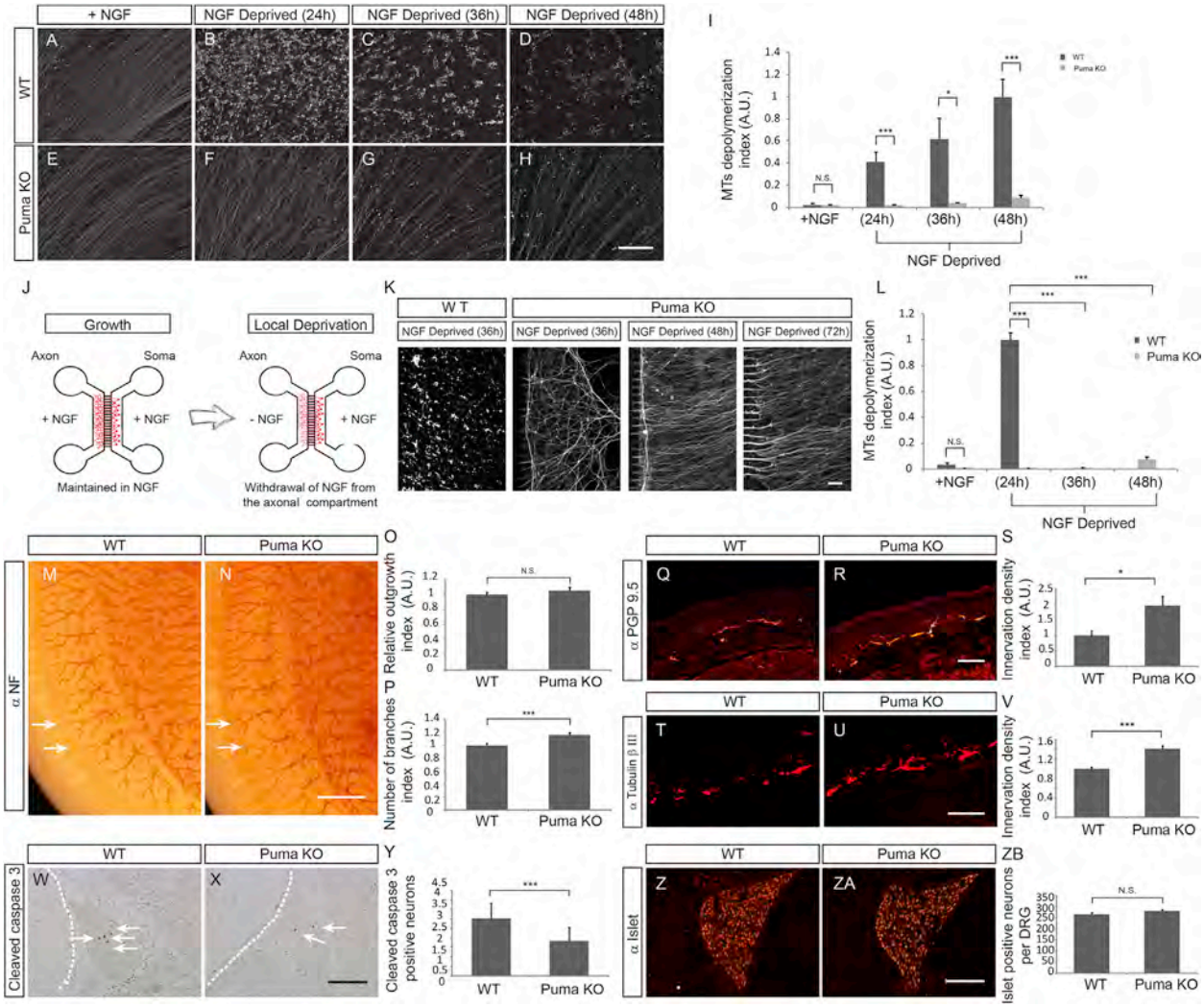

Figure 6. Genetic Ablation of *Puma* Protects Axons from Degeneration upon NGF Deprivation and Induces Developmental Skin Hyperinnervation

(A–I) DRG explants from *Puma* KO embryos (E–H) or their WT littermates (A–D) were cultured for 48 hr in NGF-containing medium. They were then either supplied with (A and E) or deprived of (B–D and F–H) NGF for an additional 24 hr (B and F), 36 hr (C and G), or 48 hr (D and H) and then immunostained for tubulin βIII. As shown in Figure 1, axonal microtubules of WT neurons were depolymerized and degraded following NGF withdrawal (B–D). In contrast, *Puma* KO neurons were protected against breakdown of axonal microtubules after NGF deprivation (F–H). Microtubule depolymerization index (mean ± SEM) was calculated for each condition and genotype (I) (t test; ***$p < 0.001$, *$p < 0.05$, n.s.).

(J) Schematic illustration of the microfluidic chamber model allowing local deprivation and axon-selective degeneration.

(K and L) *Puma* KO and WT neurons were maintained in NGF (5 days in vitro [DIV5]) and immunostained for tubulin βIII (K). Local NGF deprivation induces breakdown of the axonal microtubules in WT neurons, as can be seen from the punctuated pattern of the microtubules. In contrast, axonal breakdown of microtubules in the *Puma* KO neurons was inhibited even 72 hr after local NGF deprivation. Microtubule depolymerization index (mean ± SEM) was calculated for each condition and genotype (L) (t test; ***$p < 0.001$, n.s.).

(M–P) Whole-mount NF staining of E12.5 *Puma* KO embryos and their WT littermates, showing the peripheral nervous system growth pattern. The relative axonal outgrowth of *Puma* KO DRG spinal nerves does not differ from that of their WT littermates, but they exhibit a small, but significant, increase in branching (M and N, arrows). Relative outgrowth index (O) and axonal branches index (P). Error bars represent means ± SEM (t test; ***$p < 0.001$; n.s., n = 11).

(Q–V) Peripheral axons adjacent to the skin were analyzed in E15.5 embryos with anti-PGP9.5 antibody (Q–S) or anti-tubulin βIII antibody (T–V). In *Puma* KO embryos, sensory axons hyperinnervated the skin (R and U) compared to their WT littermates (Q and T). Innervation density index (mean ± SEM) was calculated from 5 embryos (40 sections each) for each genotype (S and V) (t test; *$p < 0.05$, ***$p < 0.001$).

(W–Y) Caspase-3 activation is reduced in DRG neurons in E15.5 *Puma* KO embryos. The numbers of cleaved Caspase-3-positive neurons at E15.5 in the DRGs of *Puma* KO embryos (X) are lower than in those of their WT littermates (W). The number of cleaved Caspase-3-positive neurons (means ± SEM) was calculated from 8 embryos (20 section each) of each genotype (Y) (t test; ***$p < 0.001$).

(Z–ZB) There is no significant effect of Puma KO on the number of Islet1-positive sensory neurons in E15.5 DRG: compare WT (Z) and *Puma* KO (ZA). The number of Islet1-positive neurons (means ± SEM) was counted in 8 embryos (20 sections each) of each genotype (ZB) (n.s.). Scale bars 100 μM (A–H, K, W, X, Z, and ZA), 50 μM (Q, R, T, and U), and 0.5 μM (M and N).

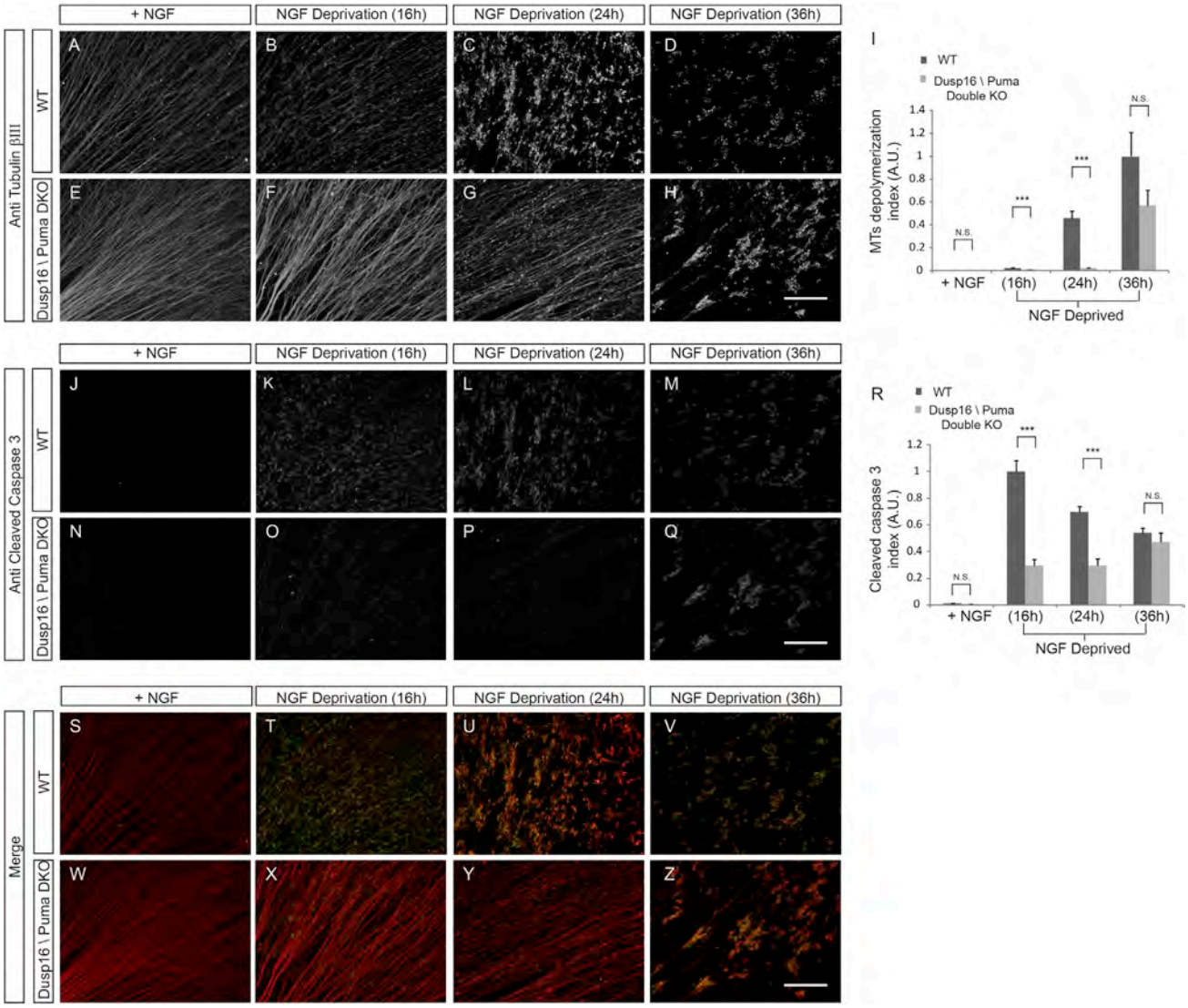

Figure 7. Co-ablation of *Puma* and *Dusp16* Delays the Activation of Caspase-3 and Axonal Degeneration

DRG explants from wild-type embryos (A–D, J–M, and S–V) or their *Dusp16*/*Puma* double KO littermates (E–H, N–Q, and W–Z) were cultured for 48 hr in NGF-containing medium. The neurons were then either supplied with (A, E, J, N, S, and W) or deprived of NGF for an additional 16 hr (B, F, K, O, T, and X), 24 hr (C, G, L, P, U, and Y), or 36 hr (D, H, M, Q, Y, and Z) and then immunostained with antibodies against tubulin βIII (A–H) and active Caspase-3 (J–Q). When deprived of NGF, the axonal microtubules of WT neurons were depolymerized and degraded, as seen from the punctuated pattern of anti-tubulin βIII staining, and active Caspase-3 is detected in the axons (S–V). In contrast, in *Dusp16*/*Puma* double KO neurons, breakdown of the axonal microtubules was inhibited and activation of axonal Caspase-3 was delayed (W–Z). Microtubule depolymerization index (mean ± SEM) was calculated for each condition and genotype (I) (t test; ***$p < 0.001$, n.s.). Cleaved Caspase-3 index (mean ± SEM) was calculated for each condition and genotype (R) (t test; ***$p < 0.001$, n.s.). Scale bar, 100 μM.

projections to the footpad's toes revealed striking complete elimination of the axons in the *Dusp16* KO that was not rescued by co-ablation with *Puma* (Figures S4K–S4O). These results suggest that Dusp16 limits the normal program of DRG neuron cell death and axonal elimination and is essential for axonal preservation. In agreement with our in vitro results, these in vivo findings indicate that Puma is a key player, but not the sole player, in the developmental axonal elimination program, and its ablation attenuated the pace of axonal loss in the *Dusp16* KO in vivo.

DISCUSSION

The results of this study show that DRG sensory neurons induce a transcriptional program in response to loss of trophic signal. Our results provide evidence that this program contains components that both promote ("accelerators") and inhibit ("brakes") cell death and axonal elimination and that these opposing regulators coordinate to produce physiological innervation during normal development (Figure 9). Therefore, the soma does not control the degeneration of axons in an all-or-nothing response

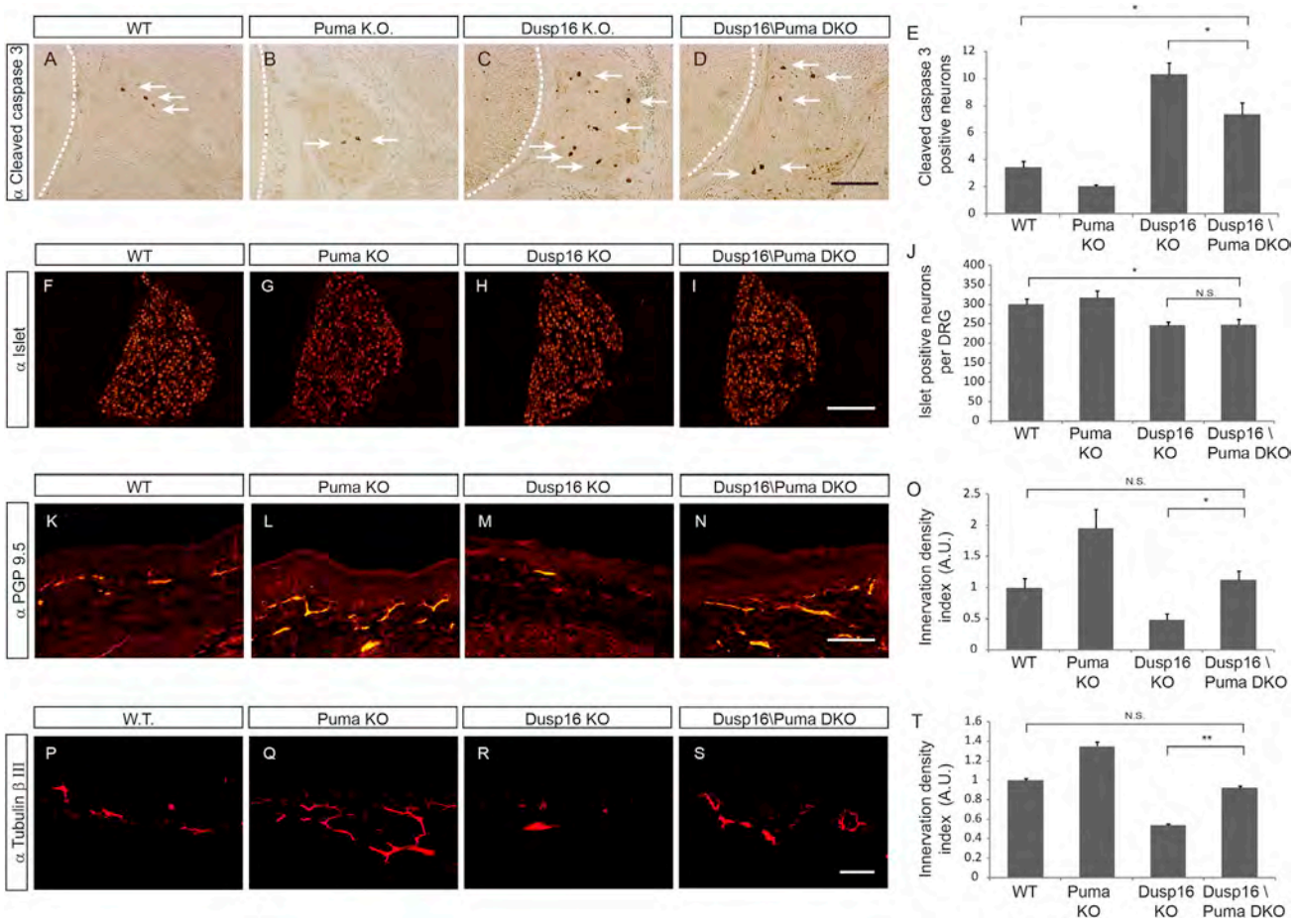

Figure 8. *Dusp16/Puma* Double KO Embryos Have Fewer Neurons but Normal Skin Innervation by Sensory Axons

(A–E) Number of cleaved Caspase-3-positive cells at E15.5 in the DRGs of WT (A), *Puma* KO (B), *Dusp16* KO (C), and *Dusp16/Puma* double KO mice (D). In the Dusp16/Puma double KO mice (D), there is increase in the Caspase-3-positive cells in comparison to their WT littermates (A). Cleaved Caspase-3-positive neurons (means ± SEM) were counted in sections from 3 to 5 embryos (40 sections each) of each genotype (E) (t test; *$p < 0.05$).

(F–J) Number of cleaved Islet1-positive neurons at E15.5 in the DRGs of WT (F), *Puma* KO (G), *Dusp16* KO (H), and *Dusp16/Puma* double-KO mice (I). The *Dusp16/Puma* double KO mice (I) at E15.5 exhibit fewer Islet1-positive neurons than their WT littermates (F). Islet1-positive neurons (means ± SEM) were counted from 4 embryos (40 sections each) of each genotype (t test; *$p < 0.05$, n.s.) (J).

(K–T) Analysis of peripheral axons adjacent to the skin labeled with anti-PGP9.5 (K–O) or anti-tubulin βIII (P–T) antibodies. Innervation in the *Dusp16/Puma* double KO embryos (N and S) does not differ from that of their WT littermates (K and P). Innervation density index (mean ± SEM) was calculated from 4 embryos (40 sections each) of each genotype (O and T) (t test; *$p < 0.05$, **$p < 0.01$, n.s.). Scale bars, 100 μM (A–D, F–I, and K–N) and 50 μM (P–S).

but rather sets the pace of degeneration through integration of this transcriptional program. In principal, signaling from additional pathways might regulate this program and stimulate or inhibit the degeneration response. Previous studies have identified NGF-induced genes that preserve the axons under normal conditions (Tasdemir-Yilmaz and Segal, 2016). Our work uncovers Dusp16 as a new brake on the degenerative response once this process is initiated. In the absence of Dusp16, axons degenerate more rapidly in response to trophic deprivation in vitro. In vivo, Dusp16 null peripheral axons show reduced branching and target innervation early in development and are completely eliminated by E17.5. This developmental axonal loss parallels increased cell death. Importantly, cell death in the *Dusp16* KO peaked at E15.5 and was largely reduced at E17.5, a stage when normal developmental cell death is completed, supporting the idea that Dusp16 acts as a brake on the normal process of cell death and axonal elimination. Neuronal loss may contribute to the axonal loss phenotype, although axonal loss was not reported in mice with greater reduction (~40%) in DRG neuronal number (Ben-Zvi et al., 2013). Moreover, co-ablation of *Puma* specifically rescues the axons early during development with no effect on neuronal number, supporting the idea that Dusp16 has an axonal protective role distinct from its effect on cell death.

Mechanistically, Dusps have been explored as negative regulators of the MAP kinase pathways (Huang and Tan, 2012). Studies of the developing nervous system have focused largely on Dusp1. Interestingly, this family member is induced by NGF withdrawal in sympathetic neurons, where it regulates cell death, and by brain-derived neurotrophic factor (BDNF) stimulation in

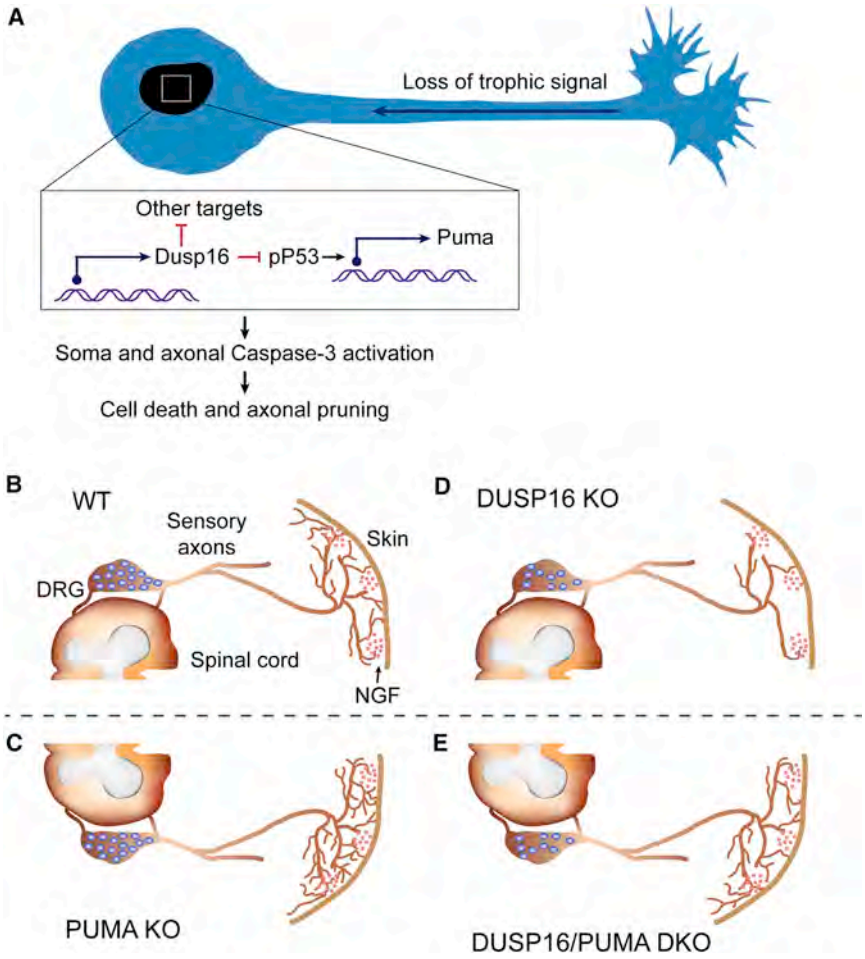

Figure 9. Coordination of Axonal Degeneration by a Transcriptional Program of Pro- and Anti-degenerative Factors

(A) Loss of trophic support stimulates a transcriptional program that controls neuronal cell death and axonal pruning through the activation of the apoptotic system. Puma promotes cell death and axonal pruning while *Dusp16* inhibits these processes through inhibition of Puma transcription and other targets.

(B–E) Neuronal number at the DRG and target innervation are set by limited amount of NGF at the target (Skin) (B). Loss of *Puma* increases the innervation density while neuronal number remains identical to the wild-type (C). In contrast, ablation of *Dusp16* cause reduction in neuronal number and target innervation compared to the wild type (D). Co-ablation of *Dusp16* and *Puma* specifically rescue the axonal innervation loss in the *Dusp16* mutant, early during development (E).

hippocampal neurons, where it controls dendritic branching (Jeanneteau et al., 2010; Kristiansen et al., 2010). In both of these cases, the prime substrate of Dusp1 was suggested to be JNK, which regulates cell death through the activation of c-Jun and, in contrast, controls dendritic branching through inhibition of the microtubule regulator stathmin-1 (Jeanneteau et al., 2010; Kristiansen et al., 2010). Dusp16 was also suggested to act as a negative regulator of JNK, as activation of JNK and p38 is prolonged in the immune system of the same *Dusp16* KO mouse that we used in this study (Niedzielska et al., 2014; Zhang et al., 2015). However, our studies of *Dusp16* KO DRGs failed to detect any enhanced phosphorylation of JNK following trophic withdrawal, of its prime substrate, c-Jun, or of p38. In contrast, we detected enhanced phosphorylation of the pro-apoptotic transcription factor p53 on Ser15, which stimulates its transcriptional activity and induces Puma expression. In the p53 KO neurons, Puma induction after trophic deprivation was strongly reduced. Surprisingly, we have not detected axonal protection in neurons from the *p53* KO mice in response to trophic withdrawal. These results argue that, on the background of *p53* KO, the basal level or minimal induction of Puma is sufficient for axonal degeneration. This may be due to the upregulation of other apoptotic/degenerative pathways or due to parallel reduction in p53-dependent anti-apoptotic genes. Indeed, previous work has shown that p53 plays an anti-apoptotic function in a model of serum withdrawal from fibroblasts (Lassus et al., 1996).

Our findings reveal strong axonal protection by Puma. Importantly, co-ablation of *Puma* and *Dusp16* delayed the rapid in vitro axonal degeneration response of the *Dusp16* KO neurons and rescued the peripheral axons early during development in vivo. These results suggest that factors other than Puma promote axonal degeneration and these are under the regulation of Dusp16 as well. A recent report suggested that Puma activates a soma-derived signal that is distinct from Puma itself (Simon et al., 2016). Using our in vitro axonal purification system, we detected Puma in the axons following trophic withdrawal, suggesting that Puma acts locally within the axon. The reasons for this difference from the prior report are not clear, but we note that the axonal purification systems are not identical. Currently available reagents only allow biochemical detection of Puma. Generation of reagents that will allow in situ detection of Puma, both in vitro and in vivo, may help resolve this issue. Regardless, both studies identify Puma as a critical regulator of axonal degeneration in vitro. Importantly, our study provides supporting evidence for this function in vivo with the following two observations. First, *Puma* KO mice show developmental target hyperinnervation early during development. Second, ablation of *Puma* on the background of the *Dusp16* KO mice specifically rescues the axonal innervation phenotype without affecting the cell death phenotype of *Dusp16* KO mice early in development.

Developmental axonal pruning, injury-induced axonal degeneration, and dying back neurodegenerative diseases share common pathways, although distinct signaling pathways have also been found (Neukomm and Freeman, 2014; Pease and Segal, 2014; Yaron and Schuldiner, 2016). Comparison of two

microarray datasets of injured neurons in the PNS and the CNS with our RNA-seq analysis identified Dusp16 and Puma as unique shared elements. Moreover, Dusp16 is upregulated in the hippocampus of ischemic mice (Wang et al., 2011). Therefore, in addition to their role in developmental axon pruning, Dusp16 and Puma may also play a role in neuronal fate decisions under pathological conditions.

EXPERIMENTAL PROCEDURES

Mouse Strains

The *Dusp16* KO mouse strain (RRID: MGI:5581506) was previously described (Niedzielska et al., 2014). *Puma* KO mice (RRID: IMSR_JAX:011067) (Villunger et al., 2003) and *p53* KO mice (RRID: IMSR_JAX:002101) (Jacks et al., 1994) were purchased from the Jackson Laboratory. All animal experiments followed protocols approved by The Weizmann Institute of Science Institutional Animal Care and Use Committee.

Explant Culture

Dorsal root ganglion explants of E13.5 mice were aseptically removed and cultured on poly-D-lysine (PDL)/laminin-coated plates. The explants were grown in neurobasal (NB) medium supplemented with 2% B-27, 1% glutamine, 1% penicillin-streptomycin, and 25 ng/mL mouse NGF 2.5S (Alomone Labs; N-100) for 48 hr before treatments. For NGF deprivation, the medium was exchanged for medium lacking NGF and containing 0.1 μg/mL rabbit anti-NGF neutralizing antibodies (Alomone; AN-240), unless otherwise is specified.

RNA Sample Preparation

DRG explants were grown, as described above, in the presence of 50 ng/mL of mNGF 2.5S (Alomone; N-100) for 36 hr. NGF deprivation was performed without medium exchange by the addition of a high concentration of anti-NGF (1.2 μg/mL) neutralizing antibodies (Alomone; AN-240). RNA was isolated after 1, 3, and 6 hr of NGF deprivation and from the control after 6 hr (without the addition of neutralizing antibodies) using QIAGEN RNeasy Plus Micro Kit (QIAGEN) according to the manufacturer's protocol. In brief, cells were lysed, homogenized, and loaded on a genomic DNA (gDNA) eliminator column. After removal of genomic DNA, RNA was purified using RNeasy spin columns. RNA quantity and purity were determined by optical density measurements of $OD_{260/280}$ and $OD_{230/260}$ using a NanoDrop spectrophotometer. Structural integrity of the total RNA was assessed with the Agilent 2100 Bioanalyzer using the Agilent Total RNA Nano Chip assay (Agilent Technologies). Seven independent replicates of RNA purification from each condition were collected and pooled for each time point.

Axonal Preparation

Cell culture inserts (1 μm pore size) adequate for a 6-well plate were coated on both sides with PDL/laminin. The inserts were placed upright in a 6-well plate, each well containing 2 mL of medium with 50 ng/mL of NGF. The inner side of the insert was filled with 1 mL of medium with 12.5 ng/mL of NGF. DRG explants were placed within the inserts and grown as described above, allowing axons, but not cell bodies, to pass through the pores and grow on the lower surface of the insert (Figure 2J). For NGF-deprivation experiments, the medium was exchanged for a medium lacking NGF but containing 0.1 μg/mL rabbit anti-NGF neutralizing antibodies (Alomone; #AN-240). Axonal material was scraped and collected from the lower surface of the insert while the DRG material was collected from the inner side of the insert.

Microfluidic Cultures

DRGs from E13.5 mice were aseptically removed and pelleted in Hank's balanced salt solution (Biological Industries) for 10 min and dissociated with 5% trypsin at 37°C for 2 min. The trypsin was neutralized with 10 mL of L15 medium supplemented with 5% fetal calf serum. The cells were then centrifuged at 2,800 rpm at 21°C for 4 min and resuspended in NB medium supplemented with B-27, glutamine, and 12.5 ng/mL NGF. The dissociated neurons were cultured on the PDL/laminin-coated microfluidic chambers and grown for 5 days as described (Cusack et al., 2013).

Immunohistochemistry

Embryos were fixed for 24 hr in 4% formaldehyde and stained as described (Maor-Nof et al., 2013).

Whole-Mount NF Staining

E12.5 mouse embryos (*Dusp16*, *Puma* KO, and WT littermates) were stained as described (Yaron et al., 2005).

Statistical Methods

Data represent mean ± SEM unless otherwise noted. Pairwise analyses were conducted by two-tailed Student's t tests (unpaired unless otherwise noted; see figure legends). The distribution of intersect lengths was performed by bootstrap test, and analyses were conducted using Microsoft Excel or R. Significance is indicated at the figure legends.

ACCESSION NUMBERS

The accession number for the RNA sequencing data reported in this paper is GEO: GSE72129.

SUPPLEMENTAL INFORMATION

Supplemental Information includes Supplemental Experimental Procedures, four figures, and one table and can be found with this article online at http://dx.doi.org/10.1016/j.neuron.2016.10.061.

AUTHOR CONTRIBUTIONS

A.Y. and M.M.-N. designed the study. M.M.-N., E.R., H.S.S., and V.U. performed experiments and data analyses. C.R. prepared tissue sections. A.N. wrote the quantifications algorithms.

D.L. performed the bioinformatics analysis. R.L. generated the Dusp16 KO line. A.Y. supervised research. A.Y. and M.M.-N. wrote the initial manuscript draft. All authors approved the final version.

ACKNOWLEDGMENTS

We thank the A.Y. lab members for advice and criticism, Moshe Oren for discussions and reagents, Varda Rotter for reagents, Eran Perlson for help with the microfluidics devices, Vladimir Kiss for help with the confocal microscopy, Ella Doron-Mandel for help with the real-time PCR, Zohar Schoenmann for assistance with the model, Ron Rotkopf for excellent statistical assistance, and Michael Fainzilber and Oren Schuldiner for critically reading the manuscript. This work was supported by funding to A.Y. from the Israel Science Foundation (873/14), The Legacy Heritage Biomedical Science Partnership of the Israel Science Foundation (1171/12), The Minerva Foundation, The Maurice and Vivienne Wohl Biology Endowment, and The Estate of Lola Asseof. A.Y. is an incumbent of the Jack & Simon Djanogly Professorial Chair in Biochemistry.

Received: August 18, 2015
Revised: June 15, 2016
Accepted: October 20, 2016
Published: November 23, 2016

REFERENCES

Aloyz, R.S., Bamji, S.X., Pozniak, C.D., Toma, J.G., Atwal, J., Kaplan, D.R., and Miller, F.D. (1998). p53 is essential for developmental neuron death as regulated by the TrkA and p75 neurotrophin receptors. J. Cell Biol. *143*, 1691–1703.

Andreassi, C., Zimmermann, C., Mitter, R., Fusco, S., De Vita, S., Saiardi, A., and Riccio, A. (2010). An NGF-responsive element targets myo-inositol

monophosphatase-1 mRNA to sympathetic neuron axons. Nat. Neurosci. *13*, 291–301.

Ben-Zvi, A., Sweetat, S., and Behar, O. (2013). Elimination of aberrant DRG circuitries in Sema3A mutant mice leads to extensive neuronal deficits. PLoS ONE *8*, e70085.

Chen, M., Maloney, J.A., Kallop, D.Y., Atwal, J.K., Tam, S.J., Baer, K., Kissel, H., Kaminker, J.S., Lewcock, J.W., Weimer, R.M., and Watts, R.J. (2012). Spatially coordinated kinase signaling regulates local axon degeneration. J. Neurosci. *32*, 13439–13453.

Courchesne, S.L., Karch, C., Pazyra-Murphy, M.F., and Segal, R.A. (2011). Sensory neuropathy attributable to loss of Bcl-w. J. Neurosci. *31*, 1624–1634.

Cusack, C.L., Swahari, V., Hampton Henley, W., Michael Ramsey, J., and Deshmukh, M. (2013). Distinct pathways mediate axon degeneration during apoptosis and axon-specific pruning. Nat. Commun. *4*, 1876.

Gerdts, J., Summers, D.W., Sasaki, Y., DiAntonio, A., and Milbrandt, J. (2013). Sarm1-mediated axon degeneration requires both SAM and TIR interactions. J. Neurosci. *33*, 13569–13580.

Ghosh, A.S., Wang, B., Pozniak, C.D., Chen, M., Watts, R.J., and Lewcock, J.W. (2011). DLK induces developmental neuronal degeneration via selective regulation of proapoptotic JNK activity. J. Cell Biol. *194*, 751–764.

Ham, J., Babij, C., Whitfield, J., Pfarr, C.M., Lallemand, D., Yaniv, M., and Rubin, L.L. (1995). A c-Jun dominant negative mutant protects sympathetic neurons against programmed cell death. Neuron *14*, 927–939.

Harrington, A.W., and Ginty, D.D. (2013). Long-distance retrograde neurotrophic factor signalling in neurons. Nat. Rev. Neurosci. *14*, 177–187.

Huang, E.J., and Reichardt, L.F. (2001). Neurotrophins: roles in neuronal development and function. Annu. Rev. Neurosci. *24*, 677–736.

Huang, C.Y., and Tan, T.H. (2012). DUSPs, to MAP kinases and beyond. Cell Biosci. *2*, 24.

Imaizumi, K., Tsuda, M., Imai, Y., Wanaka, A., Takagi, T., and Tohyama, M. (1997). Molecular cloning of a novel polypeptide, DP5, induced during programmed neuronal death. J. Biol. Chem. *272*, 18842–18848.

Jacks, T., Remington, L., Williams, B.O., Schmitt, E.M., Halachmi, S., Bronson, R.T., and Weinberg, R.A. (1994). Tumor spectrum analysis in p53-mutant mice. Curr. Biol. *4*, 1–7.

Jeanneteau, F., Deinhardt, K., Miyoshi, G., Bennett, A.M., and Chao, M.V. (2010). The MAP kinase phosphatase MKP-1 regulates BDNF-induced axon branching. Nat. Neurosci. *13*, 1373–1379.

Kristiansen, M., Hughes, R., Patel, P., Jacques, T.S., Clark, A.R., and Ham, J. (2010). Mkp1 is a c-Jun target gene that antagonizes JNK-dependent apoptosis in sympathetic neurons. J. Neurosci. *30*, 10820–10832.

Kristiansen, M., Menghi, F., Hughes, R., Hubank, M., and Ham, J. (2011). Global analysis of gene expression in NGF-deprived sympathetic neurons identifies molecular pathways associated with cell death. BMC Genomics *12*, 551.

Kuo, C.T., Zhu, S., Younger, S., Jan, L.Y., and Jan, Y.N. (2006). Identification of E2/E3 ubiquitinating enzymes and caspase activity regulating Drosophila sensory neuron dendrite pruning. Neuron *51*, 283–290.

Lassus, P., Ferlin, M., Piette, J., and Hibner, U. (1996). Anti-apoptotic activity of low levels of wild-type p53. EMBO J. *15*, 4566–4573.

Loughery, J., Cox, M., Smith, L.M., and Meek, D.W. (2014). Critical role for p53-serine 15 phosphorylation in stimulating transactivation at p53-responsive promoters. Nucleic Acids Res. *42*, 7666–7680.

Maor-Nof, M., and Yaron, A. (2013). Neurite pruning and neuronal cell death: spatial regulation of shared destruction programs. Curr. Opin. Neurobiol. *23*, 990–996.

Maor-Nof, M., Homma, N., Raanan, C., Nof, A., Hirokawa, N., and Yaron, A. (2013). Axonal pruning is actively regulated by the microtubule-destabilizing protein kinesin superfamily protein 2A. Cell Rep. *3*, 971–977.

Mariga, A., Zavadil, J., Ginsberg, S.D., and Chao, M.V. (2015). Withdrawal of BDNF from hippocampal cultures leads to changes in genes involved in synaptic function. Dev. Neurobiol. *75*, 173–192.

Martin, D.P., Schmidt, R.E., DiStefano, P.S., Lowry, O.H., Carter, J.G., and Johnson, E.M., Jr. (1988). Inhibitors of protein synthesis and RNA synthesis prevent neuronal death caused by nerve growth factor deprivation. J. Cell Biol. *106*, 829–844.

Michaelevski, I., Segal-Ruder, Y., Rozenbaum, M., Medzihradszky, K.F., Shalem, O., Coppola, G., Horn-Saban, S., Ben-Yaakov, K., Dagan, S.Y., Rishal, I., et al. (2010). Signaling to transcription networks in the neuronal retrograde injury response. Sci. Signal. *3*, ra53.

Neukomm, L.J., and Freeman, M.R. (2014). Diverse cellular and molecular modes of axon degeneration. Trends Cell Biol. *24*, 515–523.

Niedzielska, M., Bodendorfer, B., Münch, S., Eichner, A., Derigs, M., da Costa, O., Schweizer, A., Neff, F., Nitschke, L., Sparwasser, T., et al. (2014). Gene trap mice reveal an essential function of dual specificity phosphatase Dusp16/MKP-7 in perinatal survival and regulation of Toll-like receptor (TLR)-induced cytokine production. J. Biol. Chem. *289*, 2112–2126.

Oppenheim, R.W., Prevette, D., Tytell, M., and Homma, S. (1990). Naturally occurring and induced neuronal death in the chick embryo in vivo requires protein and RNA synthesis: evidence for the role of cell death genes. Dev. Biol. *138*, 104–113.

Pease, S.E., and Segal, R.A. (2014). Preserve and protect: maintaining axons within functional circuits. Trends Neurosci. *37*, 572–582.

Piñon, L.G., Minichiello, L., Klein, R., and Davies, A.M. (1996). Timing of neuronal death in trkA, trkB and trkC mutant embryos reveals developmental changes in sensory neuron dependence on Trk signalling. Development *122*, 3255–3261.

Putcha, G.V., Moulder, K.L., Golden, J.P., Bouillet, P., Adams, J.A., Strasser, A., and Johnson, E.M. (2001). Induction of BIM, a proapoptotic BH3-only BCL-2 family member, is critical for neuronal apoptosis. Neuron *29*, 615–628.

Schoenmann, Z., Assa-Kunik, E., Tiomny, S., Minis, A., Haklai-Topper, L., Arama, E., and Yaron, A. (2010). Axonal degeneration is regulated by the apoptotic machinery or a NAD+-sensitive pathway in insects and mammals. J. Neurosci. *30*, 6375–6386.

Schuldiner, O., and Yaron, A. (2015). Mechanisms of developmental neurite pruning. Cell. Mol. Life Sci. *72*, 101–119.

Sharan, R., and Shamir, R. (2000). CLICK: a clustering algorithm with applications to gene expression analysis. Proc. Int. Conf. Intell. Syst. Mol. Biol. *8*, 307–316.

Simon, D.J., Weimer, R.M., McLaughlin, T., Kallop, D., Stanger, K., Yang, J., O'Leary, D.D., Hannoush, R.N., and Tessier-Lavigne, M. (2012). A caspase cascade regulating developmental axon degeneration. J. Neurosci. *32*, 17540–17553.

Simon, D.J., Pitts, J., Hertz, N.T., Yang, J., Yamagishi, Y., Olsen, O., Tešić Mark, M., Molina, H., and Tessier-Lavigne, M. (2016). Axon degeneration gated by retrograde activation of somatic pro-apoptotic signaling. Cell *164*, 1031–1045.

Sun, W., Gould, T.W., Newbern, J., Milligan, C., Choi, S.Y., Kim, H., and Oppenheim, R.W. (2005). Phosphorylation of c-Jun in avian and mammalian motoneurons in vivo during programmed cell death: an early reversible event in the apoptotic cascade. J. Neurosci. *25*, 5595–5603.

Tasdemir-Yilmaz, O.E., and Segal, R.A. (2016). There and back again: coordinated transcription, translation and transport in axonal survival and regeneration. Curr. Opin. Neurobiol. *39*, 62–68.

Unsain, N., Higgins, J.M., Parker, K.N., Johnstone, A.D., and Barker, P.A. (2013). XIAP regulates caspase activity in degenerating axons. Cell Rep. *4*, 751–763.

Vaghefi, H., Hughes, A.L., and Neet, K.E. (2004). Nerve growth factor withdrawal-mediated apoptosis in naive and differentiated PC12 cells through p53/caspase-3-dependent and -independent pathways. J. Biol. Chem. *279*, 15604–15614.

Villunger, A., Michalak, E.M., Coultas, L., Müllauer, F., Böck, G., Ausserlechner, M.J., Adams, J.M., and Strasser, A. (2003). p53- and drug-induced apoptotic responses mediated by BH3-only proteins puma and noxa. Science *302*, 1036–1038.

Wang, L., Zhou, C., Wang, Z., Liu, J., Jing, Z., Zhang, Z., and Wang, Y. (2011). Dynamic variation of genes profiles and pathways in the hippocampus of ischemic mice: a genomic study. Brain Res. *1372*, 13–21.

Watkins, T.A., Wang, B., Huntwork-Rodriguez, S., Yang, J., Jiang, Z., Eastham-Anderson, J., Modrusan, Z., Kaminker, J.S., Tessier-Lavigne, M., and Lewcock, J.W. (2013). DLK initiates a transcriptional program that couples apoptotic and regenerative responses to axonal injury. Proc. Natl. Acad. Sci. USA *110*, 4039–4044.

Williams, D.W., Kondo, S., Krzyzanowska, A., Hiromi, Y., and Truman, J.W. (2006). Local caspase activity directs engulfment of dendrites during pruning. Nat. Neurosci. *9*, 1234–1236.

Yaron, A., and Schuldiner, O. (2016). Common and divergent mechanisms in developmental neuronal remodeling and dying back neurodegeneration. Curr. Biol. *26*, R628–R639.

Yaron, A., Huang, P.H., Cheng, H.J., and Tessier-Lavigne, M. (2005). Differential requirement for Plexin-A3 and -A4 in mediating responses of sensory and sympathetic neurons to distinct class 3 Semaphorins. Neuron *45*, 513–523.

Yoon, B.C., Jung, H., Dwivedy, A., O'Hare, C.M., Zivraj, K.H., and Holt, C.E. (2012). Local translation of extranuclear lamin B promotes axon maintenance. Cell *148*, 752–764.

Yu, J., and Zhang, L. (2008). PUMA, a potent killer with or without p53. Oncogene *27* (*Suppl 1*), S71–S83.

Yuan, J., and Kroemer, G. (2010). Alternative cell death mechanisms in development and beyond. Genes Dev. *24*, 2592–2602.

Zhang, Y., Nallaparaju, K.C., Liu, X., Jiao, H., Reynolds, J.M., Wang, Z.X., and Dong, C. (2015). MAPK phosphatase 7 regulates T cell differentiation via inhibiting ERK-mediated IL-2 expression. J. Immunol. *194*, 3088–3095.

Neuron, Volume *92*

Supplemental Information

Axonal Degeneration Is Regulated by a Transcriptional Program that Coordinates Expression of Pro- and Anti-degenerative Factors

Maya Maor-Nof, Erez Romi, Hadas Sar Shalom, Valeria Ulisse, Calanit Raanan, Aviv Nof, Dena Leshkowitz, Roland Lang, and Avraham Yaron

Supplementary Figure 1

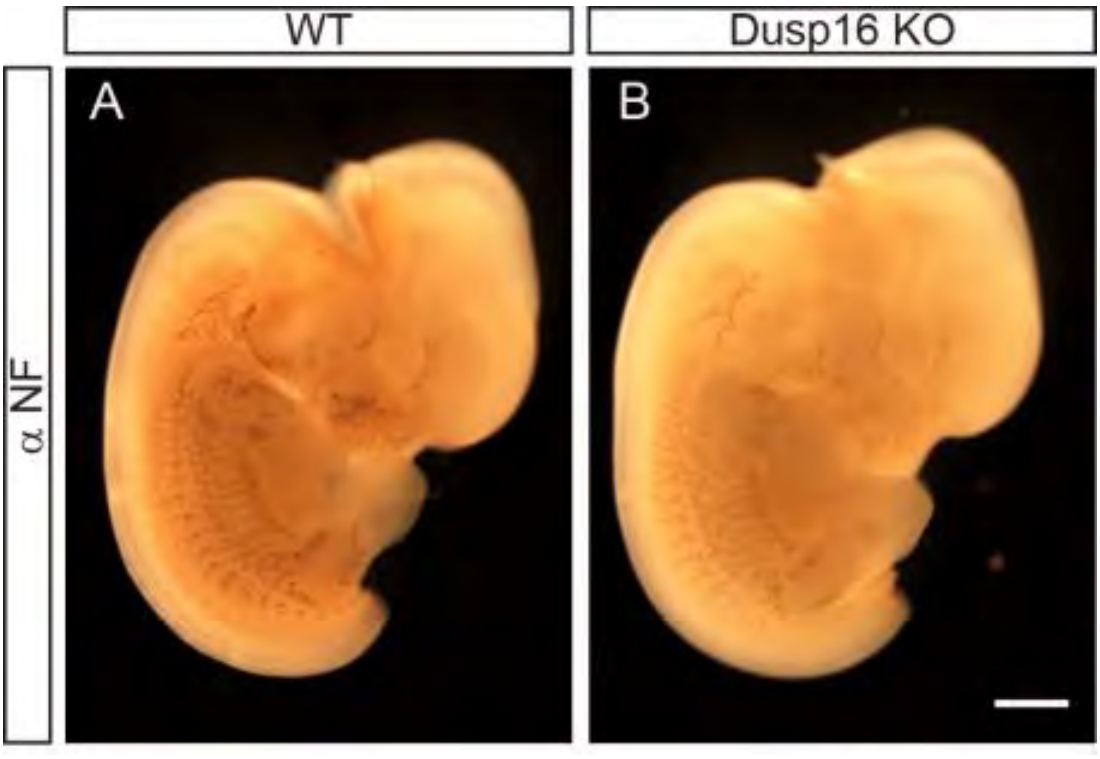

Supplementary Figure 2

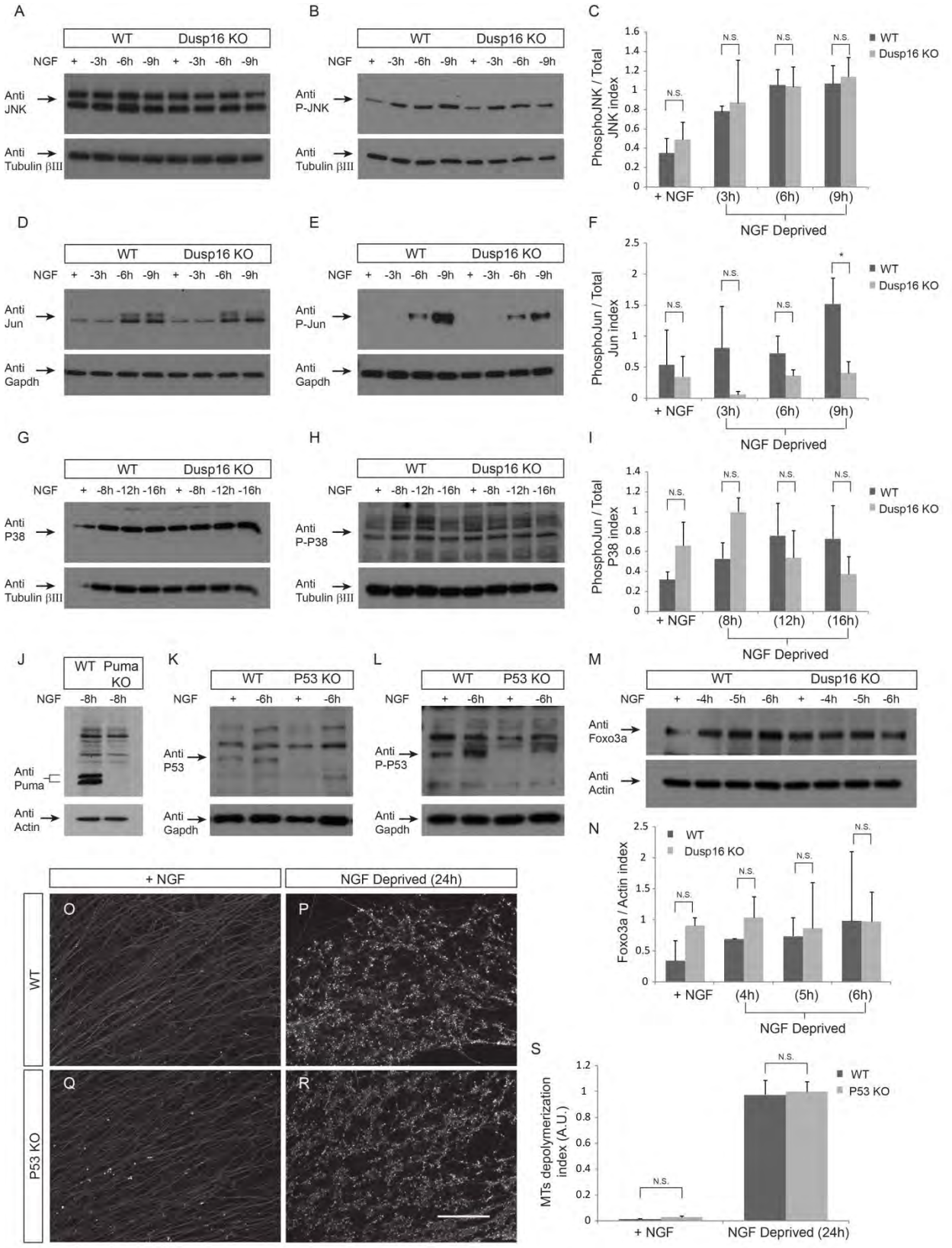

Supplementary Figure 3

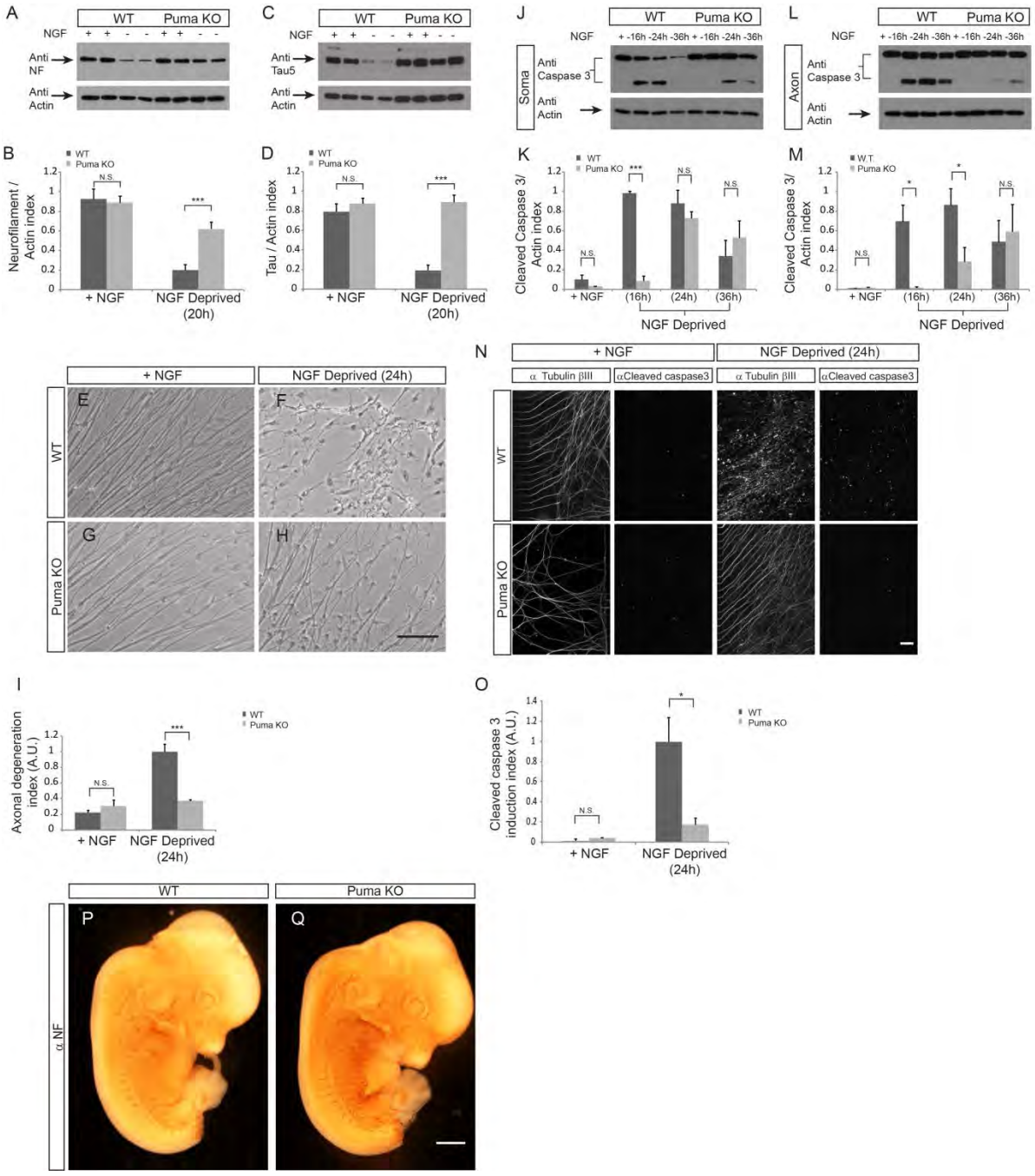

Supplementary Figure 4

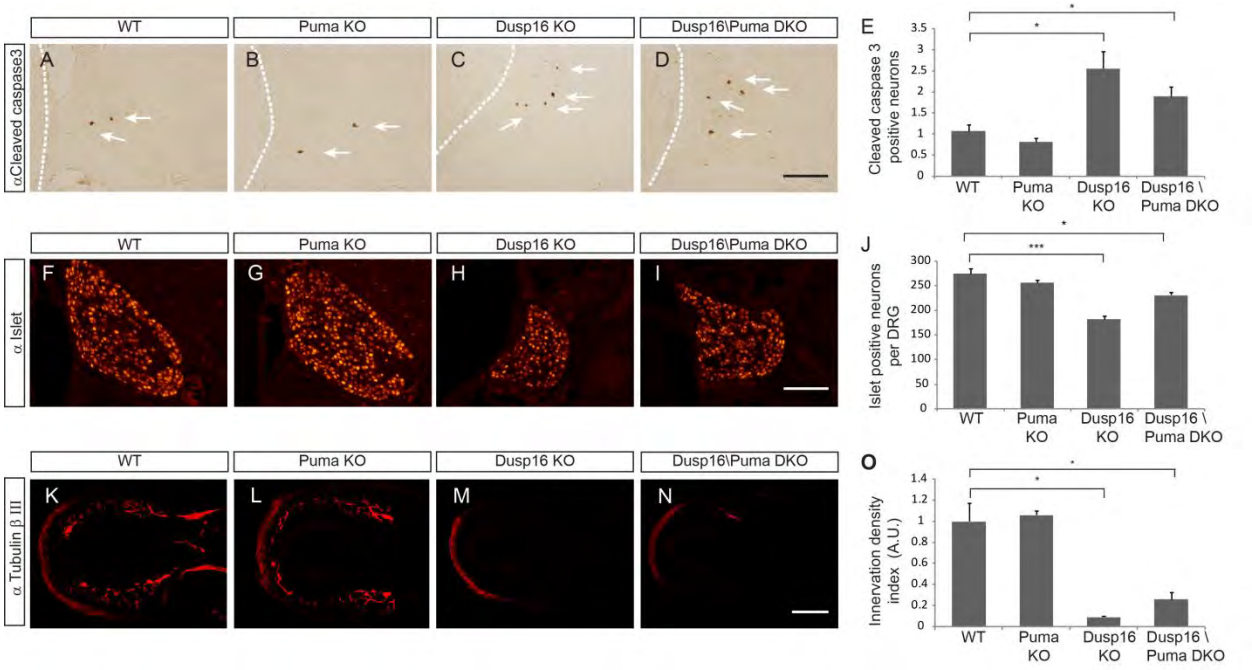

Supplementary Figure legends

Supplementary Figure 1 (related to **Figure 3) Peripheral nervous system pattern in the *Dusp16* KO embryos during early development.** Whole-mount anti-NF staining of E12.5 WT (**A**) and *Dusp16* KO embryos (**B**). Scale bar 1mM.

Supplementary Figure 2 (related to **Figure 5) Biochemical analysis of the MAP kinase pathway in the *Dusp16* KO.** DRG explants were cultured for 36 h in NGF-containing medium and deprived of NGF for the next 3, 6 and 9h or for 8, 12 and 16 h. *Dusp16* KO did not induce enhanced or earlier phosphorylation of either JNK (**A-C**), Jun (**D-F**) or p38 (**G-I**) as evaluated by immunoblots with anti-phospho-JNK, anti-phospho-Jun and anti-phospho-p38 antibodies. Moreover, reduced pJun is detectable in the *Dusp16* KO neurons 9h after NGF withdrawal (**E**). Phosphorylation levels of JNK (**C**), c-Jun (**F**) and p38 (**I**), relative to total levels for each of these proteins, were calculated from 3 different experiments (t-test; **P* < 0.05, N.S., non-significant). (**J**) Specificity of the anti-Puma antibody. DRG explants of *Puma* KO and their WT littermates were cultured for 36h in NGF-containing medium and deprived of NGF for 10h. A specific double band was detected in the WT DRGs but was not detectable in the *Puma* KO DRGs. Specificity of the anti-p53 and anti-phosphorylated p53 antibodies (**K, L**). Total levels of Foxo3a. DRG explants were cultured for 36h in NGF-containing medium and were subsequently deprived of NGF for the next 4, 5, or 6. The total level of Foxo3a in the *Dusp16* KO neurons and WT littermates controls was evaluated by immunoblot analysis **(M)**; Quantitation of total Foxo3a following NGF withdrawal was determined by immunoblots and normalized to actin (**N**). Graphs show mean ± SEM from three different experiments (t-test; N.S., non-significant, n=3). DRG explants of *p53* KO and their WT littermates were cultured for 36h in NGF-containing medium and deprived of NGF for 5h. A specific band was detected in the WT DRGs but was not detectable in the *p53* KO DRGs. p53 does not regulate axonal degeneration upon NGF deprivation. (**O–R**) DRG explants from *p53* KO embryos (**Q, R**) or their WT littermates (**O, P**) were cultured for 48h in NGF-

containing medium. They were then either supplied with (**O, Q**) or deprived of (**P, R)** NGF for a further 24h and immunostained for tubulin βIII. Upon NGF deprivation**,** the axonal microtubles of *p53* KO and WT neurons were depolymerized to a similar extent, as can be seen from the punctuated pattern of the microtubles (**N, P**). Microtuble depolymerization index (mean ± SEM) was calculated (**S**) for each condition and genotype (t-test; N.S., non-significant). Scale bar, 100 μM.

Supplementary Figure 3 (related to **Figure 6)** Genetic ablation of *Puma* protects NFs and Tau from degradation upon NGF deprivation (**A–D**). DRG explants were cultured for 48 h in NGF containing medium and then deprived of NGF for the next 20h. Degradation of NFs and Tau was evaluated by immunoblot analysis. Upon NGF deprivation, NF and Tau were greatly reduced in WT axons, whereas Tau in the *Puma* KO axons was preserved and the NF to some extent. **(B,D)** Quantitation of NF and Tau loss following NGF withdrawal was determined by immunoblots and normalized to actin. Graphs show mean ± SEM from 4 different experiments (t-test; ***$P < 0.001$, N.S., non-significant). (**E–I**) Puma ablation protects axons from degradation. DRG explants from WT (**E, F**) and *Puma* KO (**G, H**) embryos were cultured, treated as described above, and imaged by phase microscopy. (**I**) Axonal degeneration index (mean ± SEM) was calculated from each condition and genotype (t-test; ***$P < 0.001$, N.S., nonsignificant). Genetic ablation of Puma prevents Caspase-3 activation in response to global or local NGF deprivation (**J-O**). DRG explants were cultured for 36h in NGF-containing medium on cell culture inserts and were subsequently deprived of NGF for the next 16, 24, or 36h (**J–M**). Activation of Caspase-3 was evaluated by immunoblot analysis; activated (cleaved) Caspase-3 appears as a second band, below the uncleaved inactive Caspase-3 band. A clear appearance in the cleaved form is detected in both the soma and the axonal compartments of WT neurons after 16h. In the *Puma* KO, in both compartments, no cleavage of caspse-3 was detected 16h after deprivation and minor cleavage is detected at 24h in the axons. **(K, M)** Quantitation of cleaved Caspase-3 following NGF withdrawal was determined by immunoblots and normalized to actin. Graphs show mean ± SEM from three different experiments (t-test; *$P < 0.05$, N.S., non-significant). (**N, O**) Local NGF

deprivation was modeled in the microfluidic chamber. *Puma* KO and WT neurons were maintained in NGF (5 DIV) and immunostained for cleaved Caspase 3 and tubulin βIII. In the presence of NGF, no cleaved Caspase 3 is detectable either in WT or in Puma axons (left). In response to local NGF deprivation, cleaved Caspase-3 is detectable in the WT but not in the *Puma* KO axons (right). (**O**) Cleaved Caspase-3 induction index (mean ± SEM) was calculated for each condition and genotype (t-test; **P* < 0.05, N.S., non-significant). (**P, Q**)Peripheral nervous system pattern in the *Puma* KO embryos during early development. Whole-mount anti-NF staining of E12.5 WT (**P**) and *Puma* KO embryos (**Q**). Scale bar 100 μM (**E-H, N**) and 1mM (**P, Q**).

Supplementary Figure 4 (related to **Figure 8)** *Dusp16/Puma* double-KO embryos have fewer neurons and reduced skin innervation by sensory axons at a later developmental time. (**A–D**) Number of cleaved Caspase-3-positive cells at E17.5 in the DRGs of both *Dusp16* KO and *Dusp16/Puma* double-KO mice (**C, D**) are increased in comparison to their WT littermates (**A**). Cleaved Caspase-3-positive neurons (means ± SEM) were calculated from 3 to 5 embryos (40 sections each) of each genotype (**E**) (t-test; **P* < 0.05). (**F–I**) *Dusp16* KO and *Dusp16/Puma* double-KO mice (**H, I**) at E17.5 exhibit fewer Islet1 positive neurons than their WT littermates (**F**). Number of Islet1-positive neurons (means ± SEM) were calculated from 4 embryos (40 sections each) of each genotype (t-test; **P* < 0.05) (**J**). (**K−O**) Analysis of peripheral axons adjacent to the skin labeled with anti-tubulin βIII antibody. Innervation in the *Dusp16* KO and *Dusp16/Puma* double-KO embryos (**M, N**) are reduced from that of their WT littermate (**K**). Innervation density index (mean ± SEM) was calculated from 4 embryos (40 sections each) of each genotype (**O**) (t-test; **P* < 0.05, ****P* < 0.001). Scale bars, 100 μM (**A–D, F−I, K-N**).

Supplementary Table S1 (related to **Figure 2):** Pathways analysis by Ingenuity of sensory neurons transcriptome following NGF deprivation.

Experimental Procedures

Antibodies. The following antibodies and dilutions were used: tubulin β-III (Covance, MRB-435P, RRID: AB_663339, 1:1,000), tubulin β-III (R & D Systems, MAB1195, RRID:AB_357520, 1:1000), Caspase-3 (Cell Signaling; 9662, RRID:AB_10694681, 1:500), cleaved Caspase-3 (Cell Signaling, 9664, RRID:AB_331439 1:100), actin (MP Biomedicals, 691001, RRID:AB_2336056, 1:5,000), GAPDH (Millipore, MAB374, RRID:AB_21074451:1000). NF (2H3, RRID:AB_531793) and Islet1 (RRID:AB_528315) (Developmental Studies Hybridoma Bank, 1:10 and 1:1,000, respectively), Puma (Cell Signaling, 7467, RRID:AB_10829605, 1:500), Tau5 (Millipore, 577801, RRID:AB_212534, 1:1,000), JNK (Cell Signaling, 9252, RRID:AB_2250373, 1:500), H2B (Millipore, 07371, RRID:AB_310561, 1:5,000), PGP9.5 (Abcam, ab8189, RRID:AB_306343, 1:50), Fox3a (Cell signaling, 75D8, RRID:AB_836876, 1:1000), phospho JNK (Cell Signaling, 4668, RRID:AB_823588, 1:500), Jun (BD Transduction Laboratories, 610326, RRID:AB_397716, 1:500), phospho-c-Jun (Cell Signaling, 9261, RRID:AB _2130159, 1:500) p53 (Cell Signaling, 2524, AB_331743, 1:500), phospho-p53-ser15 (Cell Signaling, 9284, RRID:AB _331464, 1:400), P38 MAP Kinase (Millipore, 506123, RRID:AB _212253, 1:500), and phospho P38 MAP Kinase Thr180/Tyr182 (Millipore, MABS64, AB_10631874, 1:500). Immunoblots were developed using horseradish peroxidase-labeled donkey anti-rabbit or anti-mouse IgG and then detected with chemiluminescence. For immunofluorescence staining, anti-mouse or anti-rabbit antibodies conjugated with either Alexa 549 or Alexa 488 fluorophores were used at 1:200 (Jackson ImmunoResearch).

Library construction, sequencing, and data analysis. Total RNA was processed using the Illumina protocol. Single-end 80-bp reads were sequenced on an Illumina Genome Analyzer II. The sequence yield was between 30 and 40 million per sample. Approximately 80% of the reads were aligned to the genome build mm10 using TopHat (v2.0.10)(Trapnell et al., 2009). Genes were quantified with the program HTSeq (version 0.6.1; options -t exon -m intersection-strict -q -i gene_id) (Anders and Huber, 2010; Anders et al., 2015). Count-based differential expression analysis of RNA sequencing data was done using DESeq2 (Love et al., 2014) For gene normalization and differential expression calculations against time zero (DESeq2 parameters cooksCutoff = TRUE and independent filtering= TRUE). Differentially expressed genes were selected according to the criteria FDR ≤ 0.05 and absolute FC ≥ 1.5. The differentially expressed genes were clustered using rld values (from DESeq normalization) and the Expander tool. Heat maps and cluster profiles were plotted with Partek® Genomics Suite® software, version 6.6. Pathway analysis was performed using the IngenuitySystems IPA platform.

Quantative real time PCR. For Dusp16, Puma and GAPDH mRNA detection, 1 μg of total RNA were reverse transcribed using the iScript system cDNA kit (Bio-Rad laboratories, Hercules, California, U.S.), according to manufacturer's instructions. Dusp16 and GAPDH transcript levels were measured by TaqMan Real Time PCR, using TaqMan gene expression assay for Dusp16 (Mm00459935_m1), Puma (Mm00519268_m1) GAPDH (Mm99999915_g1) (Thermo Fisher Scientific, Waltham, MA, USA). Expression levels of the target Dusp16 mRNA were determined relative to Gapdh using the comparative Ct method to calculate changes in Ct and ultimately fold change. An average Ct value for each RNA was obtained from triplicate reactions.

Image quantification. All images were quantified using computerized algorithms except for the Cleaved Caspase 3 positive stained neurons that were manually quantified.

Axonal Quantification In Vitro and In Vivo The images of DRG explants, immmunostained for β-tubulin, were binarized such that pixels corresponding to axons converted to white while all other regions converted to black. To perform this binarization and differentiate between axons and background in the images, a localized Otsu threshold was used. The Otsu algorithm searches for a threshold that minimizes the variance sum of two or more populations in an image (Otsu, 1979). This gives an exact threshold below which all pixels are considered background. This threshold was then applied to count the number of pixels corresponding to axons in each figure, which serves as the MTs stability index. A punctuated formation of MTs was evident from the DRG explants' staining; these spots occupy only the higher gray levels in the image and appeared mostly in the NGF-deprived, and not in their corresponding controls. The MT depolymerization index was defined as the ratio of depolymerized axon pixel number to intact axon pixel number. To detect the depolymerized axons, we used an algorithm for counting all the pixels above a certain threshold. To find this threshold, we calculated the probability density function (PDF) of the sum-controlled experiments (+NGF), from which the cumulative probability density function (CDF) was extracted. The threshold was set as the value above which there were almost no pixels (less than 0.1%). Eight to twelve non-overlapping images were collected per explant. More than ten explants were analyzed for each experimental condition.

Skin Innervation Density Index Fields taken from the same area of the embryo's ventral part, such that each contained similar length of skin, were imaged. We used spectral analysis (RGB) to discriminate between axons and all other material in the image. The resulting images were then binarized above a certain threshold (as written above). Images from 45 fields were collected from each embryo and a total of 4 embryos per genotype was used. The algorithm was applied to all images counting the number of binarized pixels corresponding to axons.

Number of Islet Positive Neurons The number of neurons per DRG was calculated using an algorithm that searches circular-like shapes within the DRG area, stained with anti-islet1, using a normalized cross correlation technique with a Gaussian kernel of variable sizes. Once the kernel was applied, the algorithm found all local maxima within the resulting image, each corresponding to a neuron. The total number of neurons per each DRG was counted and neurons from all DRGs per each embryo were summarized. Images from 110 fields were collected from each embryo and a total of 4 embryos per genotype were used.

We will be happy to provide the code for this algorithm freely upon request.

Axonal Degeneration Index Following NGF-deprivation treatments, phase microscopy images revealed fragmented axons of DRG explants. The axonal degeneration index is defined as the ratio of fragmented to intact axons. Areas of fragmented axons in the image can be characterized with high frequencies in all directions (rapid gray level transitions), as opposed to other areas which are smoothed or have a directional derivative, such as the background or the axons themselves. The algorithm searches the image for areas in which the gray level derivative is high in all directions; these are counted as fragmented axons. Then, the algorithm searches for the areas that have a directional derivative (a derivative that has only one direction); these are counted as intact axons. The ratio between the two is the axonal degeneration index. The background is being filtered out, since it is smooth and has no or very small derivative. Eight to twelve non-overlapping images were collected per explant. More than 20 explants were analyzed per each experimental condition.

Relative Outgrowth Index E12.5 mouse embryos were stained using neurofilament antibody. The average length of the dorsal nerves from each DRG was calculated. Images were taken from both sides of each embryo and 4 to 16 embryos were analyzed per genotype.

Number of branches Index E12.5 mouse embryos were stained using neurofilament antibody. The relative number of branches was calculated from the number of nerves endings innervating

the dorsal skin. Images were taken from both sides of the embryos and a total of 4 to 16 embryos were used per genotype.

References

Anders, S., and Huber, W. (2010). Differential expression analysis for sequence count data. Genome Biol *11*, R106.

Anders, S., Pyl, P.T., and Huber, W. (2015). HTSeq--a Python framework to work with high-throughput sequencing data. Bioinformatics *31*, 166-169.

Love, M.I., Huber, W., and Anders, S. (2014). Moderated estimation of fold change and dispersion for RNA-seq data with DESeq2. Genome Biol *15*, 550.

Otsu, N. (1979). Threshold Selection Method from Gray-Level Histograms. Ieee T Syst Man Cyb *9*, 62-66.

Trapnell, C., Pachter, L., and Salzberg, S.L. (2009). TopHat: discovering splice junctions with RNA-Seq. Bioinformatics *25*, 1105-1111.